State of Oregon
Oregon Department of Geology and Mineral Industries
Brad Avy, State Geologist

DIGITAL DATA SERIES

2021 OREGON SEISMIC HAZARD DATABASE: PURPOSE AND METHODS

By Ian P. Madin[1], Jon J. Francyzk[1], John M. Bauer[2], and Carlie J.M. Azzopardi[1]

2021

[1]Oregon Department of Geology and Mineral Industries, 800 NE Oregon Street, Suite 965, Portland, OR 97232
[2]Principal, Bauer GIS Solutions, Portland, OR 97229

DISCLAIMER

This product is for informational purposes and may not have been prepared for or be suitable for legal, engineering, or surveying purposes. Users of this information should review or consult the primary data and information sources to ascertain the usability of the information. This publication cannot substitute for site-specific investigations by qualified practitioners. Site-specific data may give results that differ from the results shown in the publication.

WHAT'S IN THIS PUBLICATION?

The Oregon Seismic Hazard Database, release 1 (OSHD-1.0), is the first comprehensive collection of seismic hazard data for Oregon. This publication consists of a geodatabase containing coseismic geohazard maps and quantitative ground shaking and ground deformation maps; a report describing the methods used to prepare the geodatabase, and map plates showing 1) the highest level of shaking (peak ground velocity) expected to occur with a 2% chance in the next 50 years, equivalent to the most severe shaking likely to occur once in 2,475 years; 2) median shaking levels expected from a suite of 30 magnitude 9 Cascadia subduction zone earthquake simulations; and 3) the probability of experiencing shaking of Modified Mercalli Intensity VII, which is the nominal threshold for structural damage to buildings. The perceived shaking and damage potential maps and the probability of damaging shaking maps are intended to provide non-specialists with a qualitative way to assess earthquake hazards, and to see the variation of hazard across the state.

Expires: 06/30/2022

Oregon Department of Geology and Mineral Industries Digital Data Series OSHD, release 1
Published in conformance with ORS 516.030

For additional information:
Administrative Offices
800 NE Oregon Street, Suite 965
Portland, OR 97232
Telephone (971) 673-1555
https://www.oregongeology.org/
https://www.oregon.gov/DOGAMI

TABLE OF CONTENTS

GEOGRAPHIC INFORMATION SYSTEMS (GIS) DATA

OSHD Release 1_0.gdb

See appendix for a list of layers. Geodatabase is Esri® version 10.7 format. Metadata is embedded in the geodatabase and is also provided as separate .xml format files.

MAP PLATES

Plate 1. Perceived Shaking and Damage Potential, Probabilistic Earthquake Model
Highest level of shaking and damage expected with a 2% chance of occurring in the next 50 years from all earthquake sources.

Plate 2. Perceived Shaking and Damage Potential, Cascadia Subduction Earthquake Model
Median shaking levels for an ensemble of 30 Mw 9 Cascadia Subduction zone earthquakes.

Plate 3. Probability of Damaging Shaking
Probability over the next 50 years of experiencing shaking strong enough to damage weak buildings.

LIST OF FIGURES

LIST OF TABLES

EXECUTIVE SUMMARY

This report describes the methods used to prepare the Oregon Seismic Hazard Database, release 1.0 (OSHD-1.0). OSHD-1.0 is the first comprehensive collection of seismic hazard data for Oregon and contains:

- Coseismic geohazard layers that describe local ground characteristics that influence the amplification of ground shaking, liquefaction of soils, and earthquake-induced landslides,
- Maps of four common ground motion parameters using the median values for an ensemble of simulated Cascadia Subduction Zone Mw 9.0 earthquakes including amplification effects due to local soil conditions.
- Maps of four common ground motion parameters for the USGS 2018 National Seismic Hazard Map probabilistic model for a 2% probability in 50 years, including amplification effects due to local soil conditions,
- Maps of the probability of liquefaction and expected liquefaction lateral spread ground deformation for both shaking products,
- Maps of the probability of earthquake-induced landsliding and expected landslide ground deformation for both shaking products,
- Maps showing perceived shaking strength and damage potential for both shaking products (also as Plate 1 and 2),
- A map showing the probability of experiencing damaging shaking in the next 50 years, based on the probabilistic shaking (also as Plate 3).

These data are provided in Geographic Information Systems (GIS) format; see the appendix for a list of layers included.

OSHD-1.0 is an update and extension of similar data published by Madin and Burns (2013) to support the 2013 Oregon Resilience Plan prepared by the Oregon Seismic Safety Policy Advisory Commission (OSSPAC, 2013).

The coseismic geohazard layers are updated with many areas of new surficial geology mapping that have been done using high-resolution lidar topographic data, providing greatly improved accuracy and confidence in defining areas with different coseismic geohazard conditions.

The Madin and Burns (2013) report was based on a single simulation of an Mw 9.0 Cascadia Subduction Zone earthquake, which does not significantly affect eastern Oregon. OSHD-1.0 adds the shaking maps and derivative products based on the USGS probabilistic model, which provide consistent hazard information across the entire state. In addition, OSHD-1.0 uses an ensemble of 30 Mw 9 Cascadia subduction earthquake simulations recently published by the USGS (Wirth and others, 2021), which better represents the possible variability of shaking.

The liquefaction and landslide probability and ground deformation maps were calculated using the Hazus-MH loss estimation software developed by FEMA (2011). These layers were calculated in GIS for the Madin and Burns (2013) report.

The map showing the probability of experiencing damaging shaking is a new addition, based on similar maps recently produced by the USGS (Rukstales and Petersen, 2019), and is intended to help readers understand earthquake risk at their location of interest.

The new Cascadia shaking maps differ significantly from their counterparts in the Madin and Burns (2013) report, generally with higher values. This is partly due to changes in the coseismic geohazard maps, but mostly due to differences in the simulation algorithms and earthquake source parameters.

The probabilistic shaking maps have much higher values than the Cascadia ensemble maps, partly because the Cascadia maps show the median values for the 30 simulations, while the probabilistic map nominally shows the 98th percentile value for the Cascadia earthquakes it includes. The probabilistic map also includes many earthquake sources besides Cascadia and shows shaking that has a return period of 2,475 years.

The new earthquake induced landslide ground deformation map for Cascadia events has significantly lower values at the high end of the range than its counterpart in the Madin and Burns (2013) report, due to differences in the methods of calculation.

The Cascadia ensemble data can be used directly as input to Hazus-MH to run loss estimates. They can also be used for scenario-based planning for emergency response.

The probabilistic data are better suited for engineering uses like evaluating lifeline vulnerability. They can also be used cautiously for loss estimates, with the understanding that they do not represent a single simultaneous statewide event.

The perceived shaking and damage potential maps and the probability of damaging shaking maps are intended to provide non-specialists with a qualitative way to assess earthquake hazards, and to see the variation of hazard across the state.

1.0 INTRODUCTION

During the 2011 Oregon Legislative Assembly the House of Representatives passed House Resolution 3, which required the Oregon Seismic Safety Policy Advisory Commission (OSSPAC) to prepare a resilience plan for Oregon. That plan included estimates of current vulnerabilities as well as policy recommendations to address those vulnerabilities and increase the state's resilience to a great earthquake. OSSPAC completed the plan and submitted it to the legislature in February of 2013 (OSSPAC, 2013; http://www.oregon.gov/OMD/OEM/osspac/docs/Oregon_Resilience_Plan_Final.pdf). The damage estimates that underlie the plan's findings and recommendations were based on maps of the likely effects of a magnitude 9 (Mw 9) Cascadia megathrust earthquake that were prepared by the Oregon Department of Geology and Mineral Industries (DOGAMI) (Madin and Burns, 2013). The report combined bedrock ground motion models from a USGS scenario with coseismic geohazard maps based on the best available data in Oregon, largely following the methods used in the Hazus-MH loss estimation software (FEMA, 2011). The results included bedrock and site-amplified ground motions at several frequencies, coseismic subsidence or uplift, geohazard maps for soil amplification, liquefaction, and landslide susceptibility, and predictive maps of the probability and severity of liquefaction and landslide ground failure. The result was the first statewide database of coseismic geohazard information for Oregon. However, the ground shaking and ground deformation data were developed for a single Cascadia Mw 9 subduction earthquake, which represents one scenario of many possible seismic sources in Oregon.

The primary purpose of this study is to update the statewide earthquake hazard data layers provided by Madin and Burns (2013) with the best available data to produce the first comprehensive statewide earthquake hazard database, named the Oregon Seismic Hazard Database version 1.0 (OSHD-1.0). In the years since the Madin and Burns (2013) report was published many areas have new lidar-based mapping of surficial deposits. Lidar topographic data provide very high-resolution maps that allow for accurate identification and mapping of surficial geologic units, which are most important for defining localized earthquake hazards. In addition, Wirth and others (2021) recently developed new models of Cascadia subduction earthquake shaking.

In addition to updating the coseismic geohazard maps with new surficial mapping and Cascadia ground motions, the OSHD adds several new products to the initial suite of hazard maps provided by Madin and Burns (2013). These include probabilistic shaking, using the 2% probability of non-exceedance in 50-year (2,475-year return period; henceforth referred to as 2% probabilistic) USGS 2018 Long-Term National Seismic Hazard Map data (Rukstales and Petersen, 2019, Petersen and others, 2019, Shumway and others, 2020). Such data are especially important because the 2% probabilistic ground motion maps give a more realistic picture of the overall hazard, particularly for areas of the state east of the Cascades where Cascadia shaking is weak and where there are many local earthquake sources. For both Cascadia and the 2% probabilistic ground motions, we have added a map showing the expected strength of shaking as instrumental intensity, which relates numeric ground motion values to the Modified Mercalli Intensity scale, which describes earthquake strength based on impacts to people and structures (Worden and others, 2012). This measure is more meaningful to the public than ground shaking parameters such as peak ground acceleration (PGA, the highest level of acceleration recorded during a real or simulated earthquake) or peak ground velocity (PGV, the highest level of ground velocity recorded during a real or simulated earthquake) both based on numeric measurements or calculated models. Finally, we include a map based on the hazard curve data for the 2% probabilistic map that shows the probability of experiencing damaging shaking in the next 50 years.

It is important to understand the distinction between the two ground shaking models used and how they differ from the model presented by Madin and Burns (2013), because the results in this OSHD are substantially different. The Madin and Burns (2013) ground shaking model was a scenario Mw 9 earthquake, calculated using a single set of parameters (width and depth of locking on subduction zone, amount of slip, etc.). It did not account for any natural variability or model uncertainty. In contrast, the new Cascadia ensemble model (Wirth and others, 2021) is a combination of 30 different Mw 9 scenarios using a range of values for the various parameters. The Cascadia ensemble model therefore both encompasses the potential variability of events and accounts for some of the uncertainty in model parameters, but it results in a range of shaking values for a given location. For this study we used the median ground motions of the 30 values, which are nominally the most likely. The most likely values are more suitable for a scenario planning exercise or loss estimation. It is important to remember that the median ± 1σ or 2σ values, which are not included here, can be much higher or lower.

The 2% probabilistic model includes shaking contributions from all potential sources, including Cascadia subduction events of all sizes, intraslab earthquakes, and crustal earthquakes both from known faults and patterns of historic seismicity. Parameters of all earthquake sources are varied using a logic tree approach that assigns probabilities to each considered value for each parameter. Like the Cascadia ensemble model, the output is a range of values called a hazard curve. The hazard curve relates the strength of shaking to its probability of occurrence at each point in the model. This is usually presented as the maximum shaking to be expected at a fixed probability level, typically a 10%, 5%, or 2% chance of occurrence over a 50-year period. It recognizes the fact that at any site, rare events may cause extreme shaking. Such information is particularly well suited to determine what shaking strength design standard a structure requires to achieve a chosen level of certainty that the structure will not be damaged or collapse in a rare event.

In simpler terms, the Cascadia ensemble model is an updated and more sophisticated version of the Madin and Burns (2013) Cascadia model. It is suitable for scenario planning and loss estimations with the understanding that these are median values. The 2% probabilistic model can be viewed as an upper limit for the level of shaking associated with an event having a low probability of occurrence. It can be used for generalized engineering, lifeline vulnerability assessment, and non-scenario-based emergency management planning, but is less suited for a scenario planning event because the levels of shaking depicted never occur simultaneously. It should be used cautiously for loss estimates, recognizing that it represents a long-term aggregate hazard, rather than any single earthquake.

This report describes the data sources and methods used to prepare the OSHD. The goal was to provide GIS data views, or maps, that were detailed enough to show geology-based variations at the scale of a neighborhood (the 30-m cell size is about the same as two typical residential taxlots) using simple GIS manipulation of existing USGS shaking data. We expect that the information will be useful to those interested in regional earthquake hazard maps and ground motion and ground failure models in Oregon as well as Hazus-MH loss estimates. These data views should give emergency managers, planners, and the public a clearer picture of the hazard in their community as well as providing regional scale reference data for engineering studies.

Section 2 of this report describes the preparation of the coseismic geohazard maps including National Earthquake Hazard Reduction Program (NEHRP) class, landslide susceptibility, and liquefaction susceptibility. Data sources are introduced and the methods for combining them into a single uniform statewide map are described. Section 3 describes the Cascadia and 2% probabilistic bedrock ground motion data and how these data were combined with the NEHRP site class data to produce site-amplified ground motion maps. The report then describes in Section 4 the methods combining the site-amplified

ground motion and coseismic geohazard maps, used to prepare the ground failure maps. Section 5 describes how the Mercalli Intensity and probability of damage maps were prepared. Section 6 discusses the differences in the data between this report and Madin and Burns (2013).

The maps have been prepared using data sources with native resolutions in the range of several kilometers to tens of meters. The GIS data described in this report are provided in an Esri® version 10.7.1 geodatabase named OSHD Release 1_0.gdb; see the appendix for a list of layers. The data are provided as raster datasets in the Oregon Statewide Lambert Conformal Conic Projection, unit: International feet. Horizontal Datum NAD 83: 2011, with a cell size of 30 m (98.4 ft). Select maps are provided as plates in Adobe® portable document format (PDF).

2.0 COSEISMIC GEOHAZARD MAPS

The coseismic geohazard maps presented in this study describe characteristics of local geology and topography that influence earthquake shaking and ground failure. They are:

- NEHRP classes—soft rock (B), dense soil or soft rock (C), stiff soil (D), and soft clay or soil (E, F) — used to calculate ground shaking amplification,
- liquefaction susceptibility classes (no susceptibility to very high susceptibility) — used to calculate liquefaction probability and ground deformation due to lateral spreading,
- landslide geologic materials classes—strongly cemented rock (A), weakly cemented rocks (B), and argillaceous rocks (C) — used to calculate a landslide susceptibility map,
- landslide susceptibility, derived from the landslide material class map and a map of topographic slope, and provided for both dry and wet soil conditions — used for landslide probability and ground deformation calculations.

The coseismic geohazard maps are based on the following types of source data (**Figure 2-1**):

- digital geologic maps derived from the most current version of the Oregon Digital Geologic Compilation (OGDC-7; Franczyk and others, 2020a) updated with recently completed lidar-based mapping,
- the most current version of the Statewide Landslide Information Database for Oregon (SLIDO-4.2; Franczyk and others, 2020b),
- recently completed or published coseismic geohazard studies (2D studies),
- older published coseismic geohazard studies that include subsurface data (3D studies).

The footprints of the various data types included in the coseismic geohazard maps are shown in the OSHD Data Source Map included in the OSHD 1.0 geodatabase.

Figure 2-1. Map showing types of source data used for the coseismic geohazard maps. Uncolored Oregon areas use data from the updated version of OGDC-7, described in section 2.1. Cooperating Technical Partnership (CTP) studies are funded by FEMA under the CTP Program. See Table 2-1 for source information.

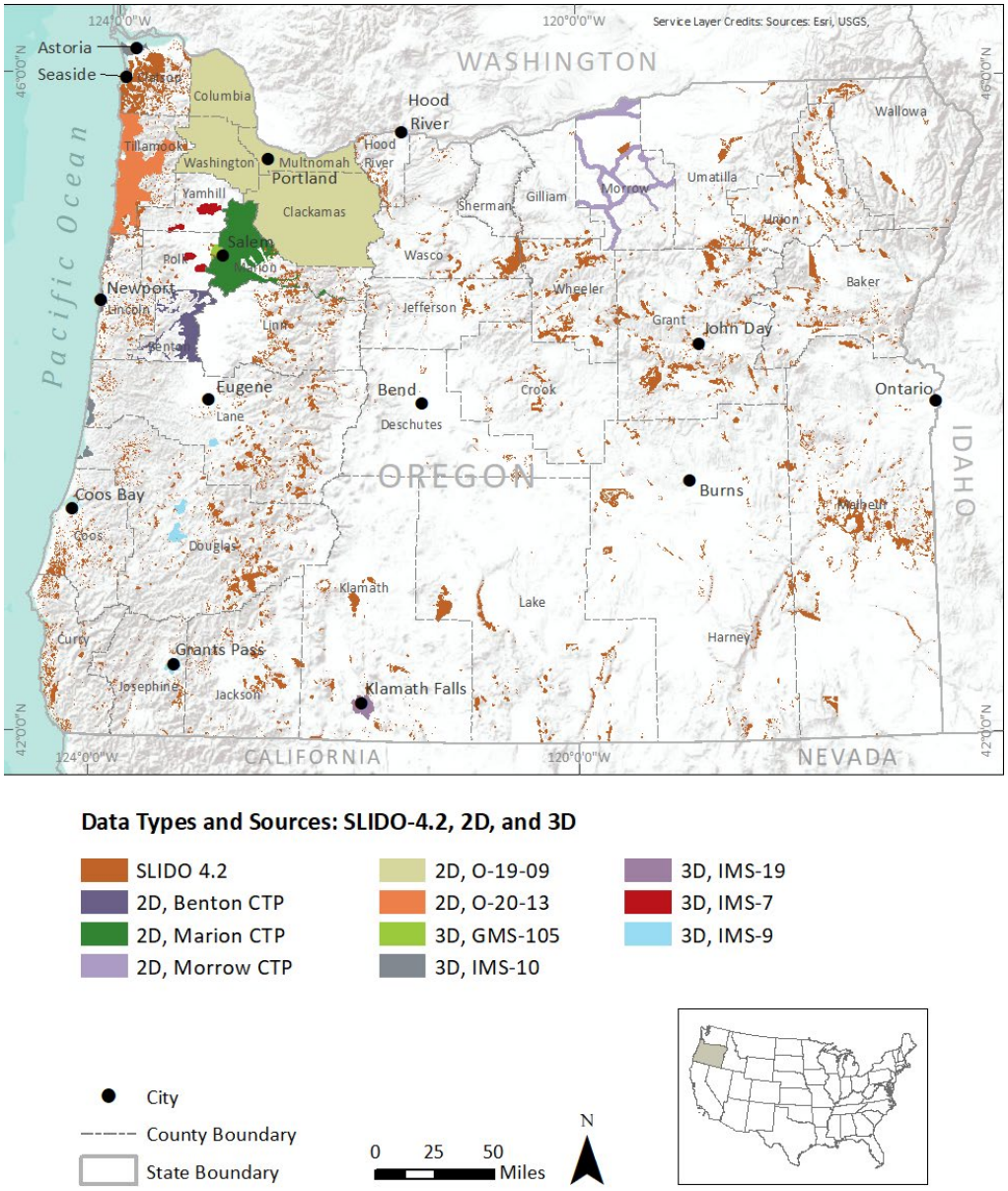

2.1 Geologic map data

To make the earthquake hazard maps as accurate as possible, we updated OGDC-7 by adding several maps that were recently published or completed but not yet published. All these new maps were prepared with lidar-based mapping of surficial geologic units at a scale of 1:8,000, which provides a level of accuracy and detail that supersedes all previous mapping. The maps that were added, along with their publication status, are presented in **Figure 2-2** and **Table 2-1**.

Figure 2-2. Published and in-preparation geologic maps that are not in OGDC-7 but are used in this study. Uncolored Oregon areas correspond to 2D, 3D, and SLIDO 4.2 data shown in Figure 2-1. See Table 2-1 for source information.

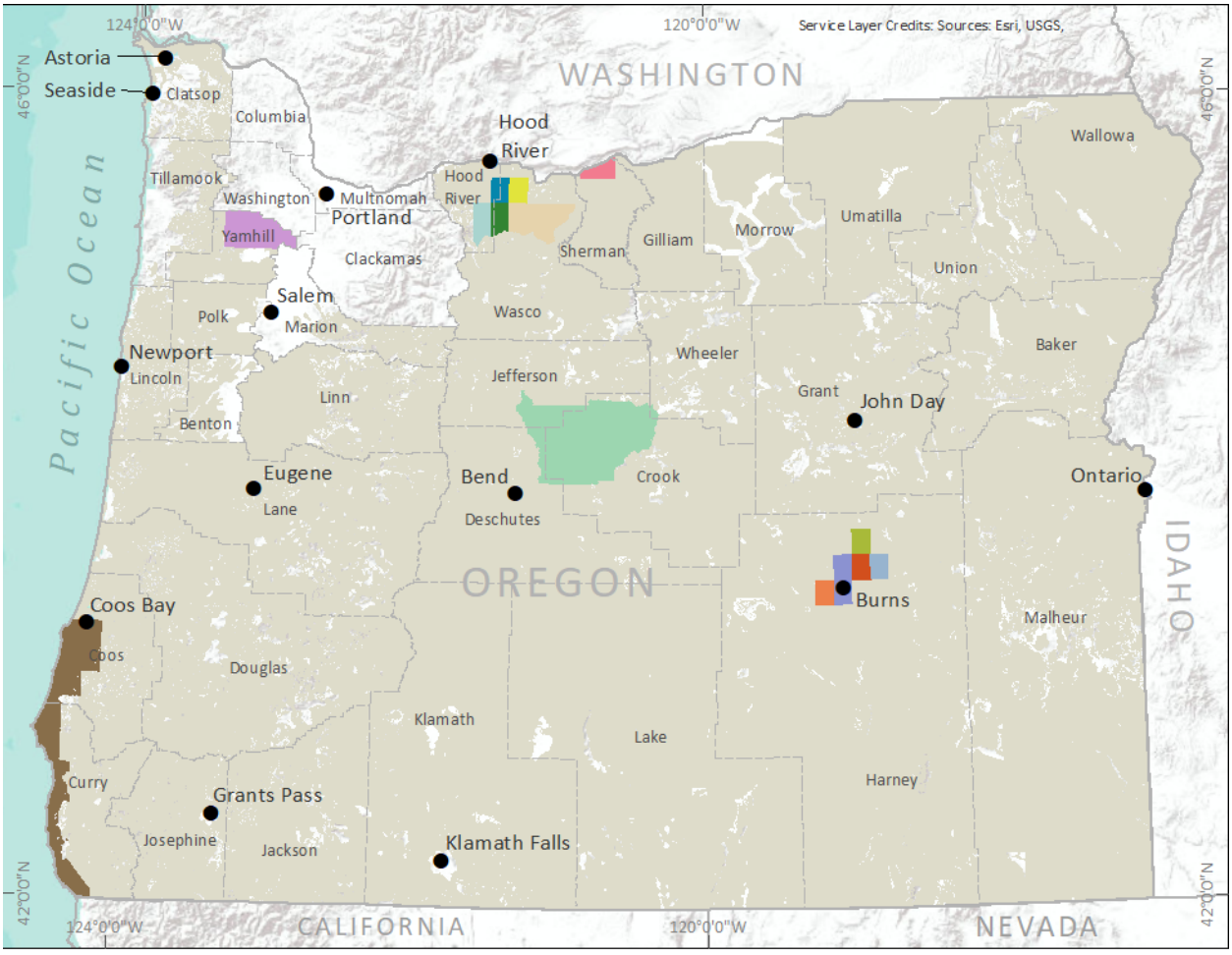

Data Sources: OGDC-7 and Geologic Studies

- OGDC-7
- Brown Creek Quadrangle
- Bulletin 108
- Fivemile Butte Quadrangle
- GMS-120
- GMS-121
- GMS-127
- GMS-123
- GMS-124
- GMS-125
- GMS-126
- Harney Quadrangle
- Ketchum Reservoir Quadrangle
- SIM-3443
- South Coast

- City
- County Boundary
- State Boundary

0 25 50 Miles

N

Table 2-1. Published and in-preparation geologic maps added to OGDC-7 for this study.

Maps	Publication Status	Reference
DOGAMI GMS-126	published	McClaughry and others, 2020a
Five Mile Butte quadrangle	in preparation	DOGAMI
DOGAMI GMS-127	published	McClaughry and others, 2021
DOGAMI GMS-124	published	Madin and McClaughry, 2019
Ketchum Reservoir quadrangle	in preparation	DOGAMI
Brown Creek quadrangle	in preparation	DOGAMI
DOGAMI GMS-123	published	McClaughry and others, 2019
DOGAMI GMS-125	published	McClaughry and others, 2020b
DOGAMI GMS-121	published	Houston and others, 2018
DOGAMI GMS-120	published	Niewendorp and others, 2018
Harney quadrangle	in preparation	DOGAMI
USGS SIM-3443	published	Wells and others, 2020
DOGAMI Bulletin 108	in preparation	McClaughry and others, in press
South Coast	in preparation	DOGAMI

For the maps that are unpublished, peer review may result in small changes to the shape or attributes of some of the geologic map polygons. The advantages of including these unpublished maps with lidar-based surficial unit mapping warrants the slight risk that some polygons will be different in their respective final map publications. In all cases these maps replace earlier maps that have surficial geology mapping of much lower resolution and accuracy. Once published, the maps will be added to the next incremental update of OGDC-7 and replace the underlying data.

2.2 Coseismic geohazard maps based on updated geology

The five coseismic geohazard maps show the following site characteristics:

- NEHRP site classes (FEMA, 2015) divide surface materials into 6 classes based on the shear wave velocity of the upper 30 m of the local geologic profile. The site classes are used to estimate the extent to which the site will amplify or attenuate ground shaking. The classes are:
    - A, Hard rock, Vs30 > 1,500 m/s,
    - B, Rock, 760 m/s < Vs30 ≥ 1,500 m/s
    - C, Very dense soil or soft rock, 360 m/s < Vs30 ≥ 760 m/s
    - D, Stiff soil, 180 m/s < Vs30 ≥ 360 m/s
    - E, Soft soil, Vs30 ≤ 180 m/s
    - F, Soil requiring site specific evaluations (for example, peat or landslide deposits)
- Hazus-MH liquefaction susceptibility classes divide surface materials based on their susceptibility to liquefaction when saturated and shaken by earthquake motions. The scale ranges from 0 (no susceptibility, for example bedrock) to 5 (very high susceptibility, for example Holocene alluvial sand deposits) and is based on Table 4 of Youd and Perkins (1978).
- Hazus-MH landslide geologic material classes divide surface materials into one of three classes of general landslide susceptibility based on Table 4-15 of Hazus-MH. The three classes are A, strongly cemented rocks; B, weakly cemented rocks; and C, argillaceous rocks.
- Hazus-MH landslide susceptibility, which combines the map of landslide geologic material class with topographic slope as described in Section 2.6.

Madin and Burns (2013) assigned NEHRP rock to soil site classes, liquefaction susceptibility classes, and landslide geologic groups to geologic units in OGDC based on factors like measured and inferred shear wave velocity, liquefaction classes from the literature, or spatial statistics of known landslides. For this study we assign values based on the Thematic Formation, Lithology, and Rock Type attributes from OGDC (**Table 2-2**). These values are based on those assigned by Madin and Burns (2013) with some significant revisions as shown in **Table 2-3**. For surficial units, values are based on the Thematic Formation attribute, modified with Thematic Lithology and in some cases geologic age. For bedrock units, the values are based on Thematic Rock Type, modified with Thematic Lithology and in some cases geographic regions or other factors (Madin and Burns, 2013). We assigned the values from **Table 2-2** to all units in the map, resulting in a statewide map of purely geology-based site classes.

The most significant changes in NEHRP site class from the Madin and Burns (2013) classifications (**Table 2-3**) are for alluvial deposits, colluvial deposits, Missoula flood deposits, and fine-grained or tuffaceous marine sedimentary rocks because they are widespread units. The changes were made to conform to the classification used for recent earthquake risk studies for the greater Portland urban area (Bauer and others, 2020; Bauer and others, 2018; Appleby and others, 2019). The change for alluvial deposits increases the hazard, because Class E soils generally amplify shaking more strongly than Class D. The changes for Missoula flood deposits decrease the hazard by reducing landslide and liquefaction susceptibility. The changes to colluvial deposits increase landslide susceptibility, whereas the changes for fine-grained or tuffaceous marine sedimentary rocks decrease coseismic landslide susceptibility.

It is important to note that we assign NEHRP site classes for geologic units with the assumption that the shear wave velocity is constant to a depth of 30 m (FEMA, 2015). In most cases, units with very low measured values (like alluvium) will overlie higher-velocity sediment or rock at depths less than 30 m. Therefore, these NEHRP class designations are conservative (likely to predict greater site amplification than would occur).

Table 2-2. NEHRP site class, liquefaction susceptibility class, and landslide geologic groups for geologic units in OGDC-7 and SLIDO 4.2. *(continued on next page)*

Surficial units (OGDC Thematic Rock Type = Sediment)					
OGDC Thematic Formation	**Note**	**OGDC Thematic Lithology**	**NEHRP Class**	**Hazus-MH Liquefaction Susceptibility Class**	**Hazus-MH Landslide Geologic Material Class**
alluvial deposits		all	E	5	B
alluvial fan deposits	Quaternary	all	D	2	B
alluvial fan deposits	pre-Quaternary	all	C	1	B
beach deposits		all	D	3	C
Bonneville Flood deposits		fine grained sediments	D	4	B
coastal terrace deposits		all	D	2	B
colluvial deposits		all	E	3	C
debris flow deposits		mixed grained sediments	D	3	C
eolian deposits		all	D	4	C
estuarine deposits		fine grained sediments	F	5	C
fan-delta deposits		coarse grained sediments	D	3	B
glacial deposits		mixed grained sediments	D	2	B
glacial outwash deposits		mixed grained sediments	D	3	B
lacustrine deposits		fine grained sediments	E	3	C
landslide deposits		mixed grained sediments	F	3	C

Surficial units (OGDC Thematic Rock Type = Sediment)					
OGDC Thematic Formation	**Note**	**OGDC Thematic Lithology**	**NEHRP Class**	**Hazus-MH Liquefaction Susceptibility Class**	**Hazus-MH Landslide Geologic Material Class**
laterite deposits		mixed grained sediments	D	1	B
loess		fine grained sediments	D	4	B
man-made fill deposits		all	F	5	C
marsh deposits		fine grained sediments	F	5	C
mine tailings		mixed grained sediments	F	5	C
Missoula flood deposits		fine grained sediments	D	3	B
Missoula flood deposits		mixed grained sediments	C	2	B
playa lake deposits		fine grained sediments	E	4	C
pluvial lake valley deposits		mixed grained sediments	D	3	B
spring chemical sediments		all	D	2	B
terrace deposits	Quaternary	all	D	2	B
terrace deposits	pre-Quaternary	all	C	1	B

Bedrock Units (OGDC-7 Thematic Rock Types Other Than Sediment)					
OGDC Thematic Rock Type	**Note**	**OGDC Thematic Lithology**	**NEHRP Class**	**Hazus-MH Liquefaction Susceptibility**	**Hazus-MH Landslide Geologic Group**
batholith rocks		all	B	0	A
intrusive rocks	west of Cascade crest	all	C	0	A
intrusive rocks	east of Cascade crest	all	B	0	A
invasive extrusive rocks		all	C	0	B
mélange rocks		all	C	0	B
metamorphic rocks	west of Cascade crest	all except serpentine	C	0	A
metamorphic rocks	east of Cascade crest	all except serpentine	B	0	A
metamorphic rocks		serpentine	C	0	C
marine volcanic rocks		all	C	0	B
marine sedimentary rocks		all	C	0	B
terrestrial sedimentary rocks		all	C	0	B
volcanic rocks	west of Cascade crest	all	C	0	B
volcanic rocks	east of Cascade crest	all	B	0	B
volcaniclastic rocks	exceptions below	all	C	0	B
volcaniclastic rocks	airfall deposits	airfall deposits	D	2	C
volcaniclastic rocks	Holocene	mudflow breccia	D	2	C
volcaniclastic rocks	pre-Holocene	mudflow breccia	C	0	B
volcaniclastic rocks	fine grained volcaniclastic sediments	fine grained sediments	D	3	B
volcanic vent deposits		all	C	0	B

SLIDO-4.2 Units					
landslide deposits			F	3	C
talus/colluvial deposits			E	3	C
alluvial/debris flow fan deposits			D	2	B

Table 2-3. Units with significant change in coseismic geohazard value. Boldface, shaded entries in columns for this study indicate a changed value.

Surficial Units (OGDC Thematic Rock Type = Sediment)							
		This Study			Madin and Burns (2013)		
OGDC Thematic Formation	OGDC Thematic Lithology	NEHRP Class	Hazus-MH Liquefaction Susceptibility	Hazus-MH Landslide Geologic Group	NEHRP Class	Hazus-MH Liquefaction Susceptibility	Hazus-MH Landslide Geologic Group
alluvial deposits	fine	E	**5**	**B**	E	4	C
alluvial deposits	coarse, mixed	**E**	**5**	**B**	D	3	C
Bonneville flood deposits	fine grained sediments	D	4	**B**	D	4	C
colluvial deposits	all	E	3	**C**	E	3	B
glacial deposits	mixed grained sediments	**D**	2	B	C	2	B
loess	fine grained sediments	D	4	**B**	D	4	C
Missoula flood deposits	fine grained sediments	D	**3**	**B**	D	4	C
Missoula flood deposits	mixed grained sediments	C	2	**B**	C	2	C
Bedrock Units (OGDC Thematic Rock Types Other Than Sediment)							
OGDC Thematic Rock Type	OGDC Thematic Lithology	NEHRP Class	Hazus-MH Liquefaction Susceptibility	Hazus-MH Landslide Geologic Group	NEHRP Class	Hazus-MH Liquefaction Susceptibility	Hazus-MH Landslide Geologic Group
marine sedimentary rocks	basin plain mudstone	C	0	**B**	C	0	C
marine sedimentary rocks	fine-grained sediments	C	0	**B**	C	0	C
marine sedimentary rocks	mudstone	C	0	**B**	C	0	C
marine sedimentary rocks	slope mudstone	C	0	**B**	C	0	C
marine sedimentary rocks	tuffaceous	C	0	**B**	C	0	C
terrestrial sedimentary rocks	all	C	0	**B**	C	0	C

2.3 Incorporation of SLIDO-4.2 data

DOGAMI recently published and incremental update to the fourth release of the Statewide Landslide Information Database for Oregon, SLIDO 4.2 (Franczyk and others, 2020b). This database contains many mapped landslide deposits that are not in OGDC-7. For this study, the newly added landslide deposits were assigned NEHRP site classes, landslide susceptibility, and landslide geologic material classes as shown in **Table 2-2**. SLIDO 4.2 deposits replace other data, or are replaced by other data as shown in **Figure 2-3** and as follows:

1. The 2D studies replace SLIDO 4.2 because they are based on recent detailed lidar-based mapping.,
2. The updated OGDC-7 data that are lidar-based replace SLIDO 4.2 unless the SLIDO-4.2 data are based on landslide inventories following the protocol of Burns and Madin (2009).
3. SLIDO 4.2 data replace all 3D studies, which used only slope for landslide susceptibility assessment.
4. SLIDO 4.2 data replace all updated OGDC-7 data that were not mapped using lidar.

2.4 Coseismic geohazard maps from other studies

We included completed maps of coseismic geohazard data from several previously published or soon to be published studies (**Table 2-4**). The "2D" data are based on assignments of coseismic geohazard classes to maps of surficial geology constructed specifically for that purpose. These maps do not factor in the effect of varying deposit thickness on site classes but are based on detailed lidar-based surficial mapping. In contrast, the "3D" data do not use lidar-derived surficial geology mapping but are instead based on models of the shear wave velocity of the upper 30 m derived from paper geologic maps of varying scales, borehole data, and locally measured shear wave velocity data. **Table 2-4** lists the studies used, and their publication status and data type; **Figure 2-1** shows the location of these studies, and **Figure 2-3** shows the order of supersedence of the various data types.

The 3D studies presented in **Table 2-4** used different classes and were converted to the current format following the method outlined by Madin and Burns (2013), shown in **Table 2-5**. Madin and Burns (2013) considered the 3D studies to be the highest quality and therefore these studies superseded all other data. However, in this update the 3D studies supersede only those maps based on the original OGDC-7 geology for the NEHRP and liquefaction susceptibility data and are themselves superseded by newer 2D studies and the lidar-based updates of OGDC-7. These newer studies are based on far more detailed and accurate surficial geology mapping using lidar and cover large areas uniformly. Using them will maintain consistency with the most recently published data. Additionally, the increased accuracy of the lidar-based mapping is of comparable value to the inclusion of the 3D study shear wave velocity models.

The 3D studies had landslide hazard classes based solely on slope from 30-m DEMs, so they are not used in preparing the final landslide geologic material class maps.

Table 2-4. Sources of site class data from other hazard studies.

Study	Reference	Status	Type
DOGAMI GMS-93	Wang and Priest, 1995	published	3D
DOGAMI GMS-105	Wang and Leonard, 1995	published	3D
DOGAMI IMS-07	Madin and Wang, 1999b	published	3D
DOGAMI IMS-08	Madin and Wang, 1999a	published	3D
DOGAMI IMS-09	Madin and Wang, 1999c	published	3D
DOGAMI IMS-10	Madin and Wang, 1999d	published	3D
DOGAMI IMS-19	Black and others, 2000	published	3D
DOGAMI O-19-09	Appleby and others, 2019	published	2D
Marion County CTP*		in preparation	2D
Benton County CTP*		in preparation	2D
Morrow County CTP*		in preparation	2D
DOGAMI O-20-13	Calhoun and others, 2020	published	2D

*Projects funded by FEMA Cooperating Technical Partnership (CTP) under 2018 mapping activity statement (MAS) 25.

Table 2-5. Assignment of site class values from published 3D studies. See Table 2-4 for publication references.

3D Publication	Publication Liquefaction Category	Liquefaction Susceptibility, This Report	Publication Amplification Category	NEHRP Class, This Report
IMS-7, -8, -9, -10	High	4	B	B
	Moderate	3	C	C
	Low	2	D	D
	None	0	E	E
IMS-19	Low	2	1	B
	None	0	2	C
	—	—	3	D
GMS-93	High	4	1	B
	Moderate	3	2	C
	Low	2	3	D
	None	0	—	—
GMS-105	0	0	1	C
	1	0	2	D
	2	3	3	E
	3	4	4	E
	4	4	—	—
	5	4	—	—

2.5 Final coseismic geohazard maps

The data for each coseismic geohazard map were assembled from the sources described above to produce a final statewide map. **Figure 2-3** provides a schematic view of how the maps were assembled and the order of supersedence of data. This order is as follows:

1. The new lidar-based 2D studies,
2. SLIDO-4 data based on landslide inventories that follow the protocol of Burns and Madin (2009),
3. The updated OGDC-7 data that are based on lidar topography,
4. All other SLIDO 4.2 data,
5. 3D studies (not used for landslide material class), and
6. portions of the updated OGDC-7 data that were not mapped using lidar.

The final vector polygon maps of each site class were then converted into rasters with a 30 m (98.4 ft) resolution, resulting in three final raster maps and are shown in **Figure 2-4**.

Figure 2-3. Flowchart for assembly of the three coseismic geohazard maps. Data that are higher on the diagram supersede data that are lower.

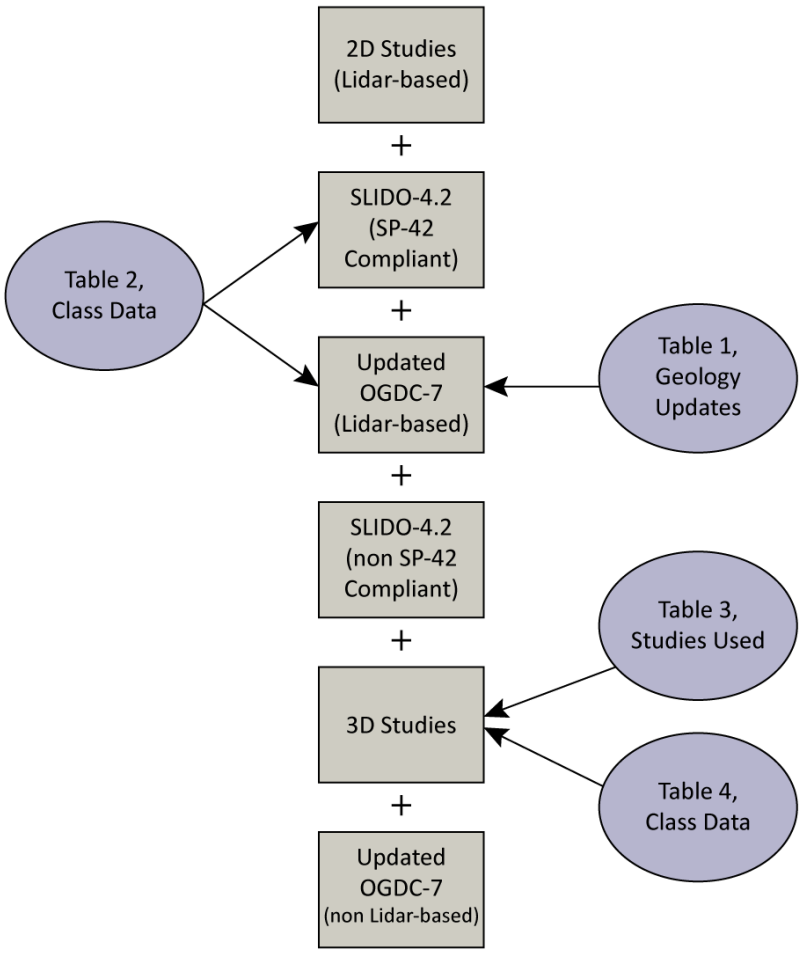

Figure 2-4. Final NEHRP site class map.

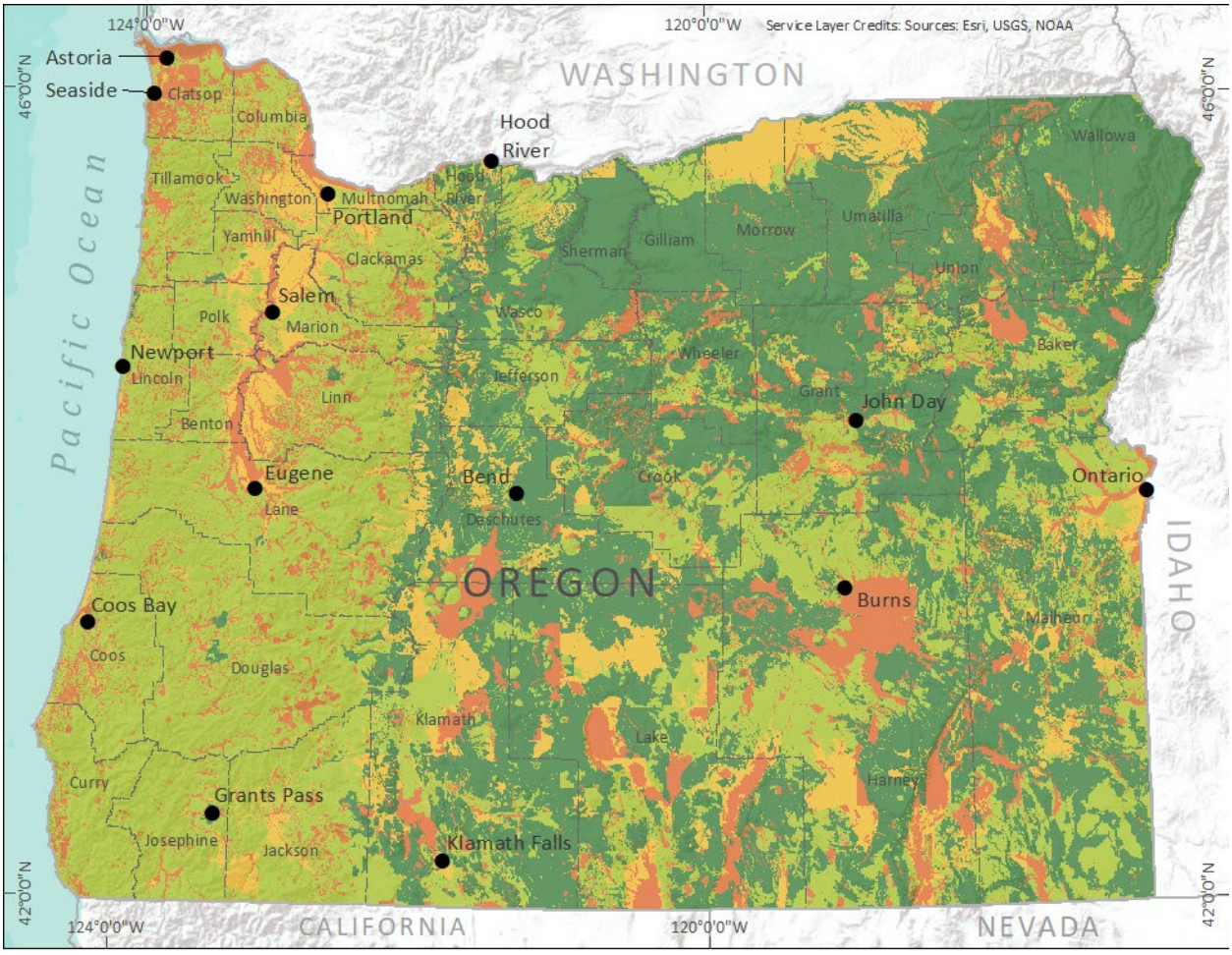

NEHRP Site Classes

- B (Rock)
- C (Dense Soils & Soft Rock)
- D (Stiff Soils)
- E/F (Soft Soils)

- City
- County Boundary
- State Boundary

0 25 50 Miles

N

Figure 2-5. Final liquefaction susceptibility class map.

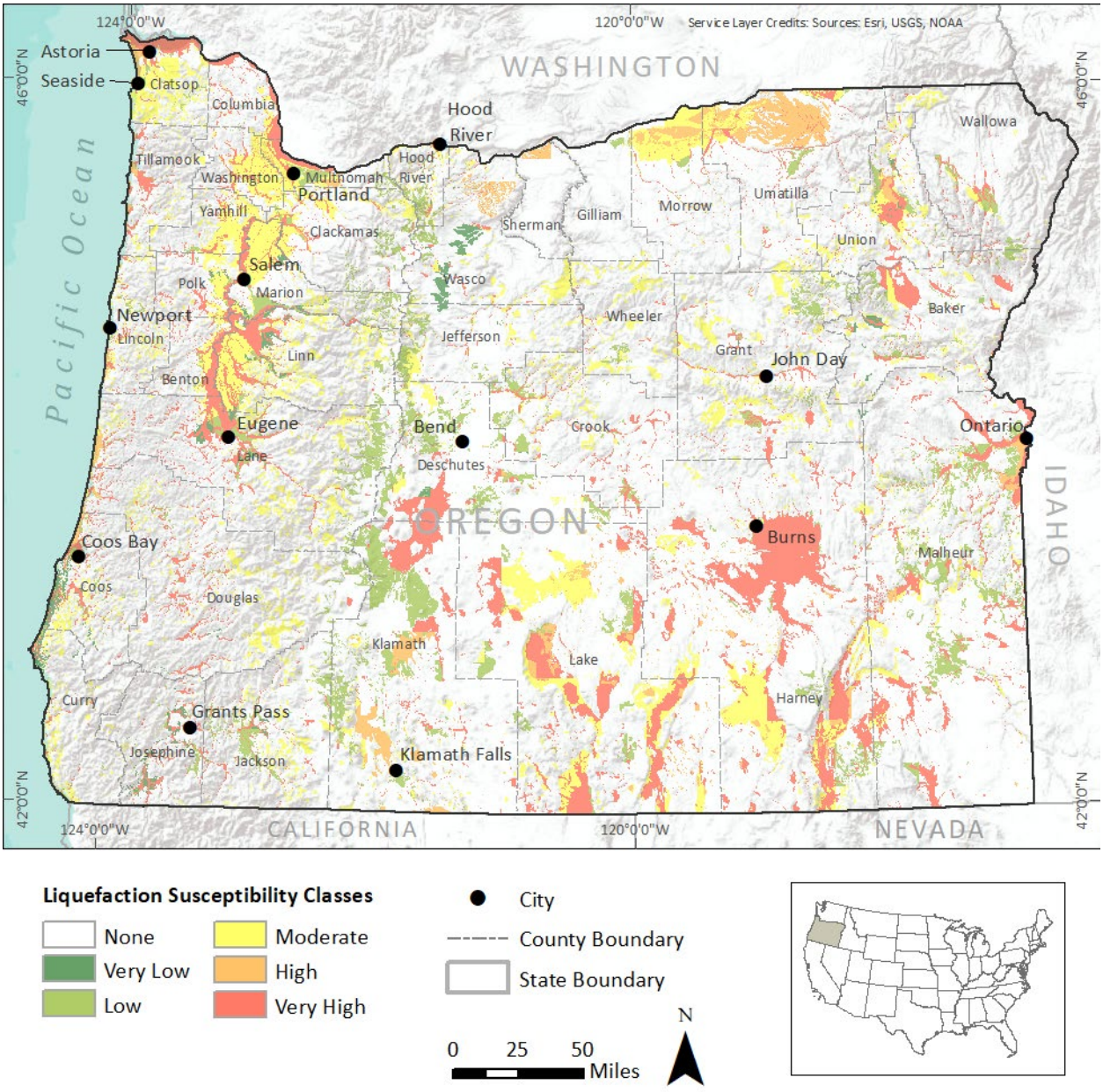

Figure 2-6. Final landslide material class map.

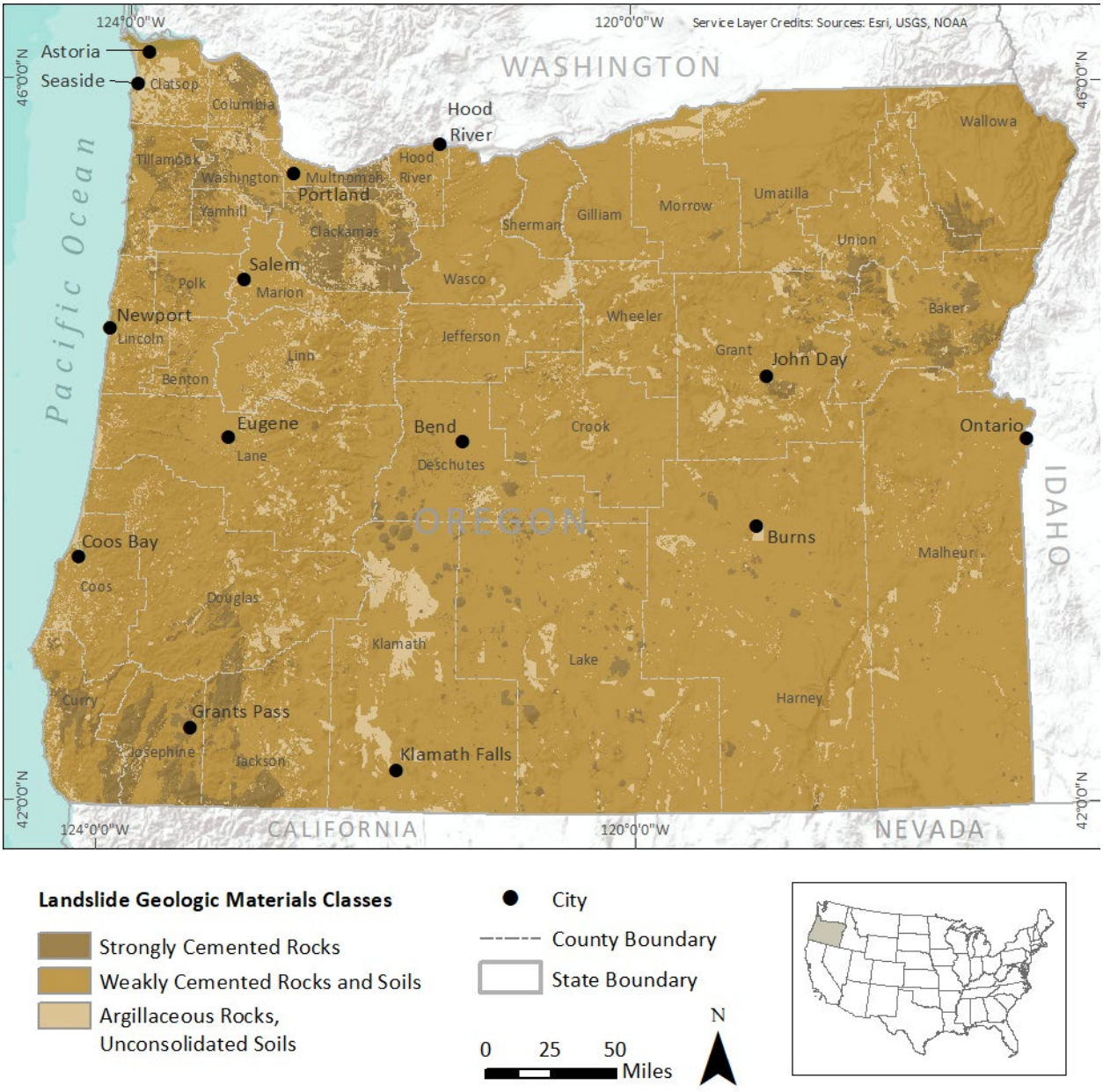

2.6 Landslide susceptibility map

We made a new statewide landslide susceptibility map for Oregon by following the methodology outlined by Madin and Burns (2013). which was based on Hazus-MH with some modifications based on the spatial distribution of mapped landslides in OGDC and SLIDO. **Table 2-6** shows the classification scheme suggested in Hazus-MH, which includes three landslide geologic material groups in a matrix with six slope classes. The matrix has 11 possible landslide susceptibility values for combinations of material group, slope, and saturated or dry conditions. **Table 2-7** shows the critical acceleration (PGA) needed to trigger landsliding at each susceptibility level,

Table 2-6. Landslide susceptibility of geologic materials (FEMA [2011] Hazus-MH Table 4-15).

Geologic Group		Slope Angle, degrees					
		0-10	10-15	15-20	20-30	30-40	>40
(a) DRY (groundwater below level of sliding)							
A	Strongly Cemented Rocks (crystalline rocks and well-cemented sandstone, $c' = 300$ psf, $\phi' = 35°$)	None	None	I	II	IV	VI
B	Weakly Cemented Rocks and Soils (sandy soils and poorly cemented sandstone, $c' = 0$, $\phi' = 35°$)	None	III	IV	V	VI	VII
C	Argillaceous Rocks (shales, clayey soil, existing landslides, poorly compacted fills, $c' = 0$ $\phi' = 20°$)	V	VI	VII	IX	IX	IX
(b) WET (groundwater level at ground surface)							
A	Strongly Cemented Rocks (crystalline rocks and well-cemented sandstone, $c' = 300$ psf, $\phi' = 35°$)	None	III	VI	VII	VIII	VIII
B	Weakly Cemented Rocks and Soils (sandy soils and poorly cemented sandstone, $c' = 0$, $\phi' = 35°$)	V	VIII	IX	IX	IX	X
C	Argillaceous Rocks (shales, clayey soil, existing landslides, poorly compacted fills, $c' = 0$ $\phi' = 20°$)	VII	IX	X	X	X	X

Table 2-7. Critical Accelerations (ac) for Susceptibility Categories (FEMA [2011] Hazus-MH Table 4-17).

Susceptibility Category	None	I	II	III	IV	V	VI	VII	VIII	IX	X
Critical Accelerations (g)	None	0.60	0.50	0.40	0.35	0.30	0.25	0.20	0.15	0.10	0.05

To make the slope class map, we made a hybrid digital elevation model of Oregon by resampling all of the available lidar topographic data to 30 m (98.4 ft) resolution, and then filling in the gaps with 30-m DEM data resampled from the from the current USGS 10-m National Elevation Database (NED) (**Figure 2-7**).

Figure 2-7. Source data for hybrid DEM.

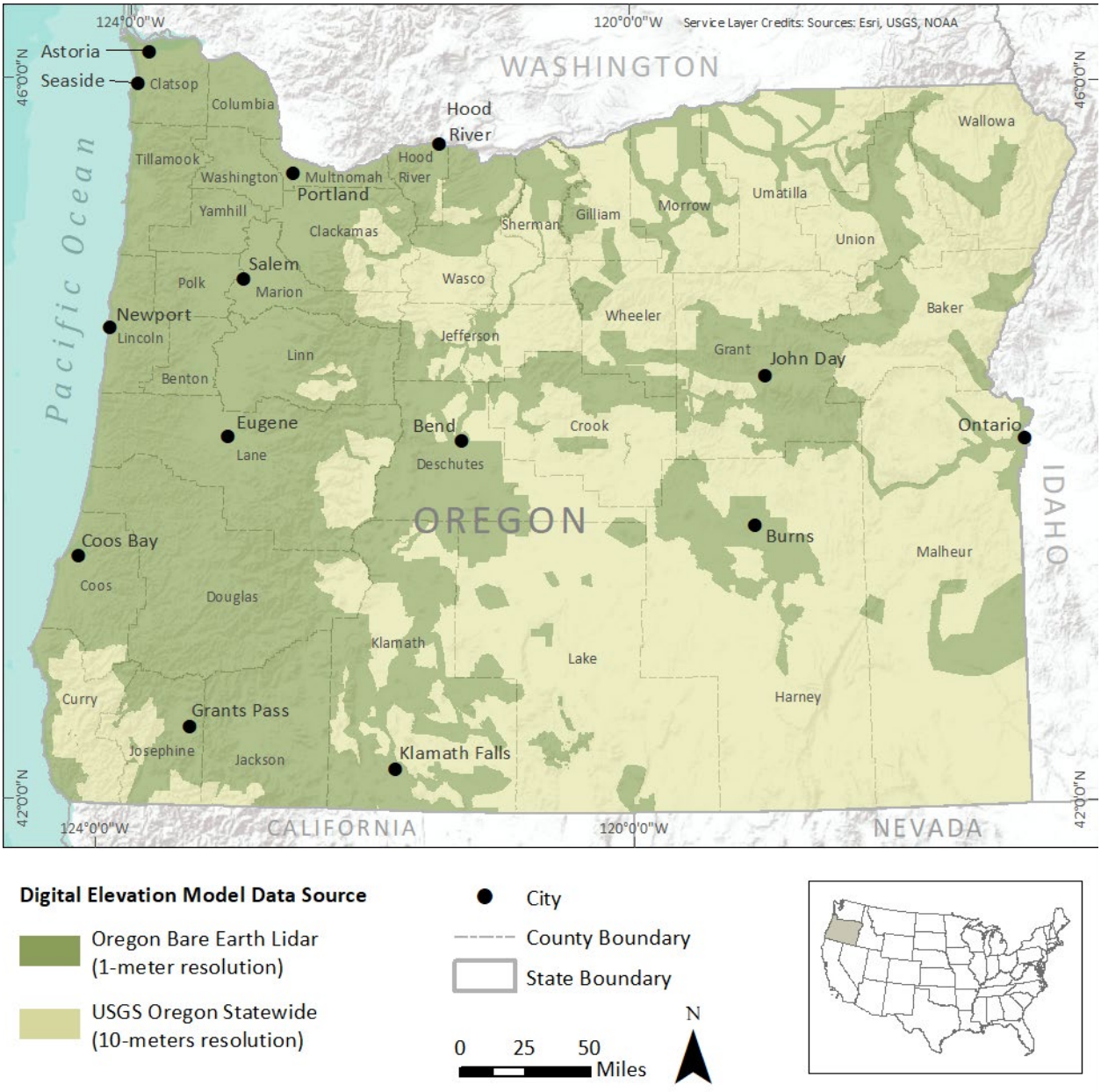

We then created a slope map from the hybrid DEM (**Figure 2-7**) and combined it with the landslide geologic group map (**Figure 2-6**) following the matrix in **Table 2-6** to create landslide susceptibility maps for both wet and dry conditions. The final landslide susceptibility class maps are shown in **Figure 2-8**.

Figure 2-8. Wet and dry condition landslide susceptibility maps derived from Hazus-MH (FEMA, 2011) methodology.

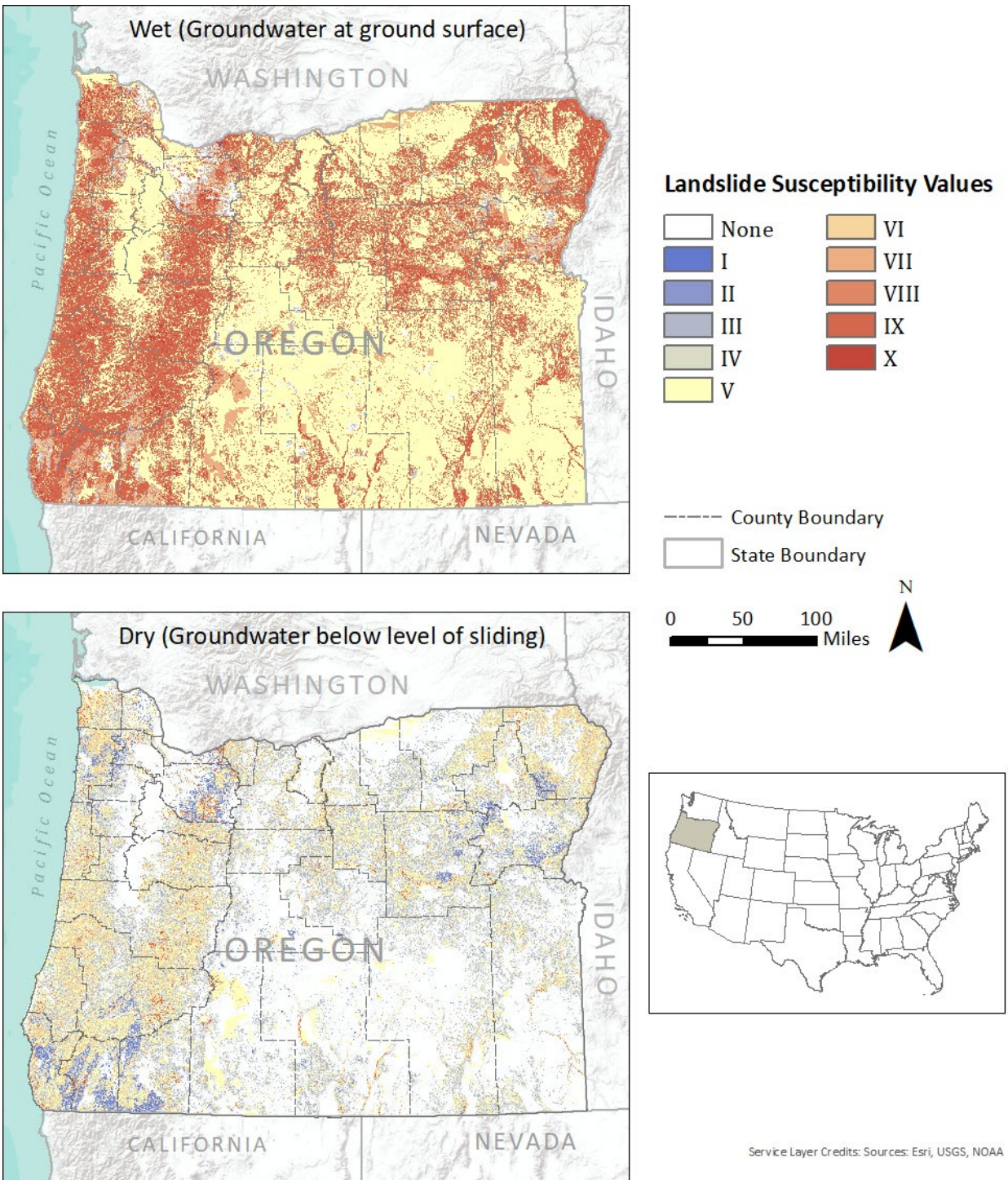

One factor that may lead this map to underestimate susceptibility is that existing landslides are at high risk for reactivation during an earthquake, and most landslides that exist in western Oregon are not represented in OGDC-7 or SLIDO-4.2 simply because they have not yet been mapped. Since 2007, DOGAMI has collected millions of acres of high-resolution lidar topography in western Oregon and has developed a protocol for creating detailed landslide inventory maps using the lidar data (Burns and Madin, 2009). Where this technique has been applied, even the best available pre-lidar landslide maps missed well over half of the landslides that could be found with lidar. In a pilot study in the Portland Metro area, Burns (2007) found that it was possible to find three times as many landslides with lidar as it was with serial stereo air photos spanning the time interval from 1936 to 2000. Therefore, it is likely that in most forested areas of Oregon, the actual number of landslides present far exceeds what is included in **Figure 2-8**. **Figure 2-9** highlights those parts of the state where DOGAMI has undertaken lidar-based landslide mapping and where the inventory can be considered complete.

Figure 2-9. Map showing areas of Oregon for which lidar-based mapping of landslides has been included in this study.

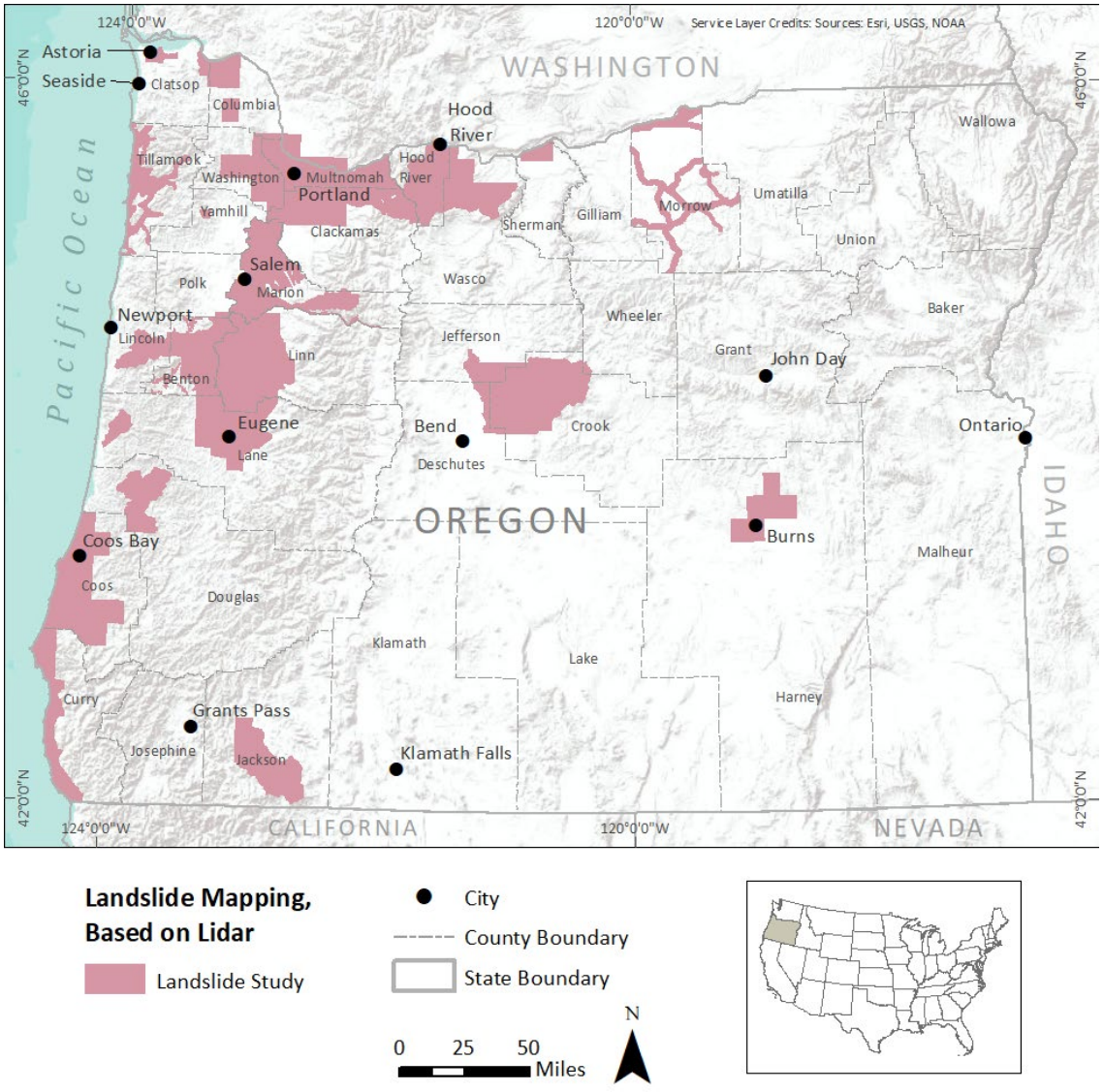

3.0 GROUND MOTION MAPS

3.1 2% probabilistic (2,475-year recurrence) ground motion maps

Earthquake ground motion estimates can be either deterministic—based on a single scenario event of some reasonably constrained magnitude, or probabilistic—incorporating weighted contributions from all plausible events and considering the full range of uncertainty in source parameters. Hence, a probabilistic model provides a better representation of the total hazard faced at a given location, while also accounting for uncertainty. Furthermore, the 2% in 50-year probability of non-exceedance (2,475-year recurrence) maps produced by the USGS are the basis for building codes and most seismic engineering design (International Code Council [ICC], 2021). We based our probabilistic ground motion maps on data from the 2018 version of the USGS National Seismic Hazard maps (Rukstales and Petersen, 2019, Shumway and others 2020). We used the USGS point data for NEHRP site classes B, C, D, and E, each of which provided data on a 0.05-degree grid (~4 km by 5.5 km or 2.5 mi by 3.4 mi) for a suite of ground motion parameters including peak ground acceleration (PGA) and spectral acceleration (SA) for 23 periods ranging from 0.01 seconds to 10 seconds. Hazus-MH requires maps of PGA, peak ground velocity (PGV), 0.3-second spectral acceleration (SA03), and 1-second spectral acceleration (SA 10). The USGS data package does not include values for PGV, so we converted the 0.5-second spectral acceleration (SA0.5) data to PGV using the Bommer and Alarcon (2006) relationship, which is:

$$PGV = SA0.5/20$$

where PGV is in centimeters per second and SA0.5 is in centimeters per second squared.

For each ground motion parameter, we interpolated the USGS point data for each of the site classes to a 30-m raster using a natural neighbor algorithm and then mosaicked them following the new NEHRP site class map, resulting in a single site-amplified map (**Figure 3-1**). The components for the four NEHRP site classes and the final mosaicked map are shown in **Figure 3-2**.

Figure 3-1. Illustration of the method used to prepare site-amplified probabilistic ground motion maps.

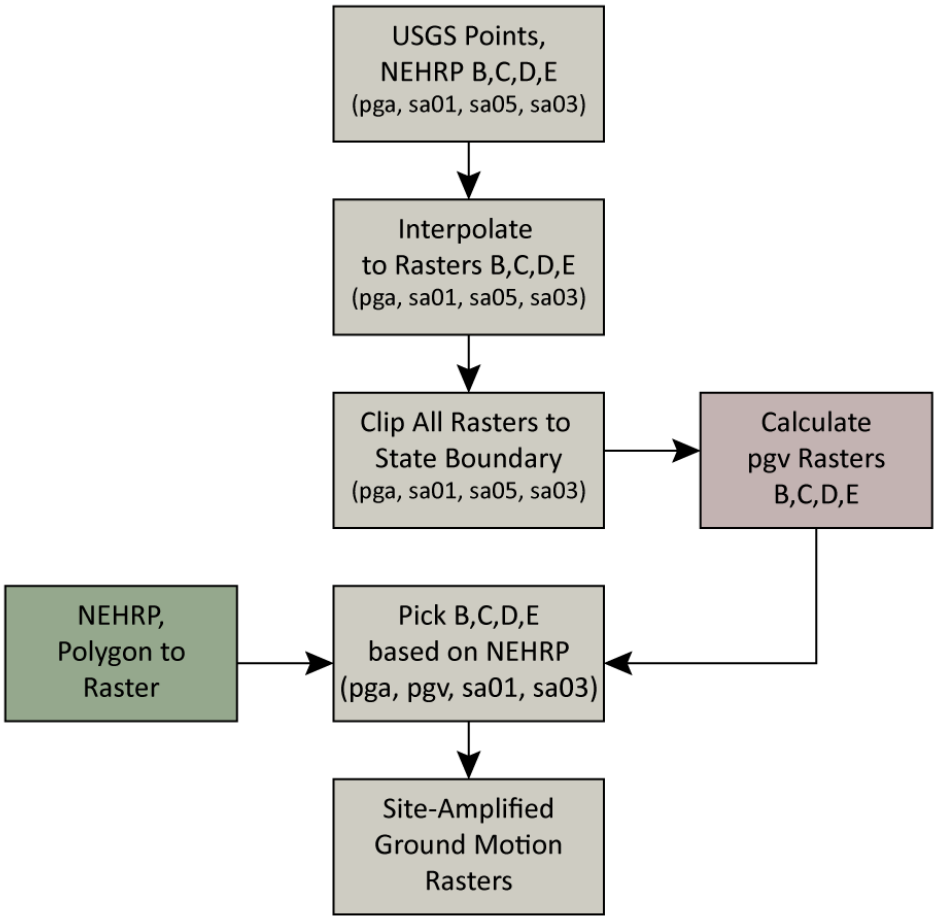

Figure 3-2. Example of site-amplified PGA map created by using NEHRP class map to pick values from ground motion rasters for each class.

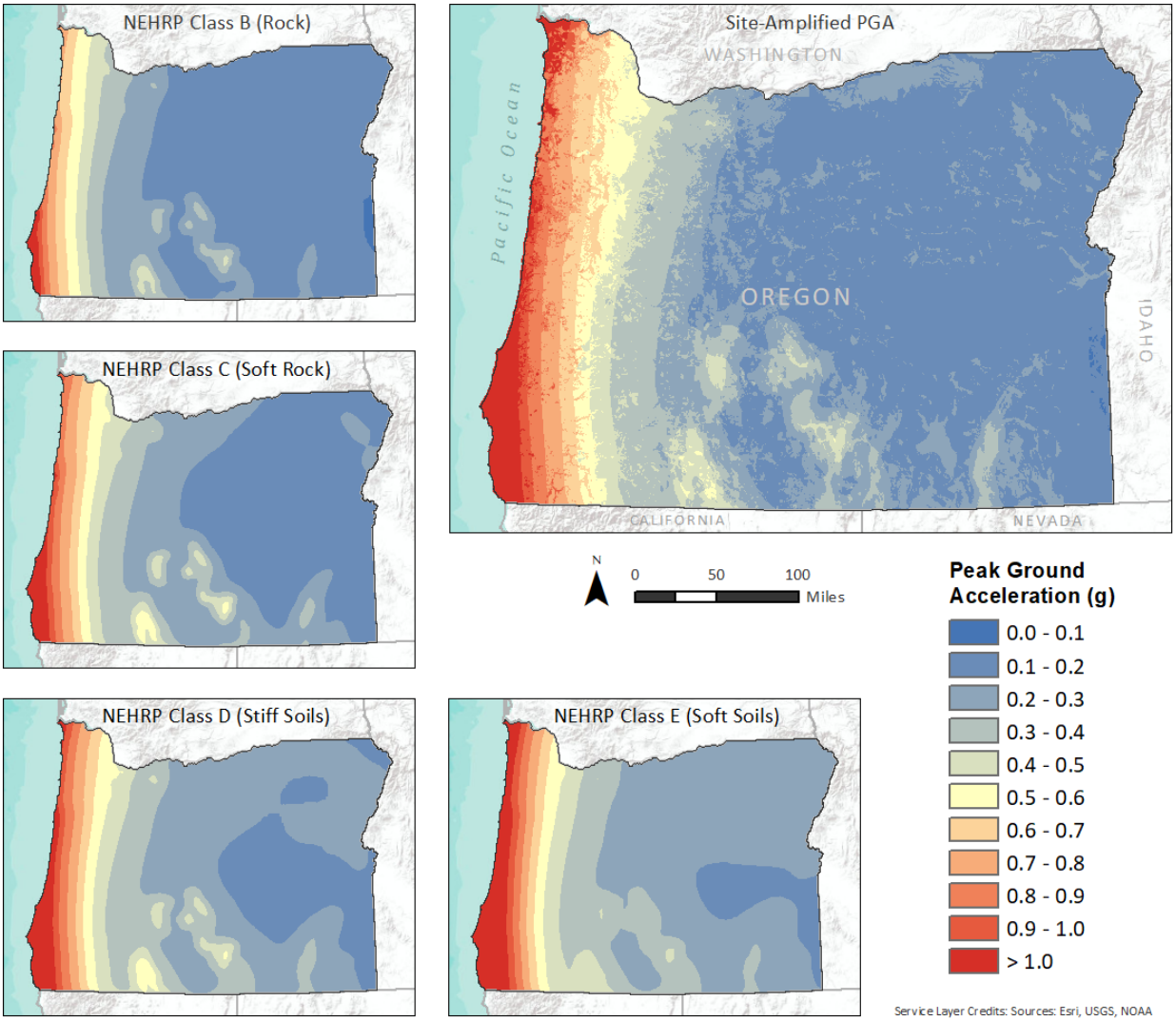

3.2 Cascadia subduction zone earthquake ground motions

Megathrust earthquakes on the Cascadia subduction zone account for most of the seismic hazard in western Oregon because of their size (Mw 8-9) and frequency (~ every 230–540 years) (Goldfinger and others, 2012, 2017). Although a wide range of possible Cascadia events are included in the 2% probabilistic ground motion maps, it can be helpful for planning and loss estimation to have a scenario Cascadia event. Madin and Burns (2013) used a single Mw 9 scenario based on the USGS Cascadia ShakeMap ground motions. In this study we use ground motions based on a new Cascadia model produced by the USGS (Wirth and others, 2021). The Cascadia Mw 9 scenario used by Madin and Burns was based on a single set of source parameters whereas Wirth and others (2021) calculated an ensemble of 30 megathrust shaking models with a range of parameters to encompass the likely variability of Cascadia rupture scenarios. The methods are described in detail by Wirth and others (2021), but the key parameters were the hypocenter location, downdip rupture limit, slip distribution and location of strong-motion-generating subevents. The results provide median, 2nd, 16th, 84th, and 98th percentile values for the ensemble for a suite of ground motion parameters. These results are semi probabilistic, in that they use a logic tree approach to weight the input values, and calculate and combine multiple models; however, unlike a true probabilistic seismic hazard map, they do not address the frequency of events or include other sources. This approach provides a ground shaking prediction that best represents the wide variability of actual Cascadia subduction earthquakes.

Wirth and others (2021) originally calculated their ground motions on a 0.02 × 0.02 degree grid (~ 5,100 ft × 7,200 ft, or 1.5 km × 2.2 km in Oregon) using the global Vs30 map of Heath and others (2020) In order to provide better resolution and take advantage of the new NEHRP site class map developed for this project, E.A. Wirth and A. Grant (written commun., 2021) graciously agreed to recalculate the models on a 150-m grid using the new NEHRP site class maps to provide Vs30 values for site amplification. The data consist of 150-m resolution rasters for the median values of PGA, PGV, SA 0.3, SA 1.0, and SA 3.0, which we subsequently resampled to 30-m resolution for consistency with the other products of this database, and to facilitate their use in the landslide and liquefaction derivatives. The resulting map for the Cascadia ensemble PGA data is shown in **Figure 3-3**.

Figure 3-3. Site-amplified Mw 9 Cascadia ensemble map for PGA. Color ramp matches Figure 3-2 for comparison.

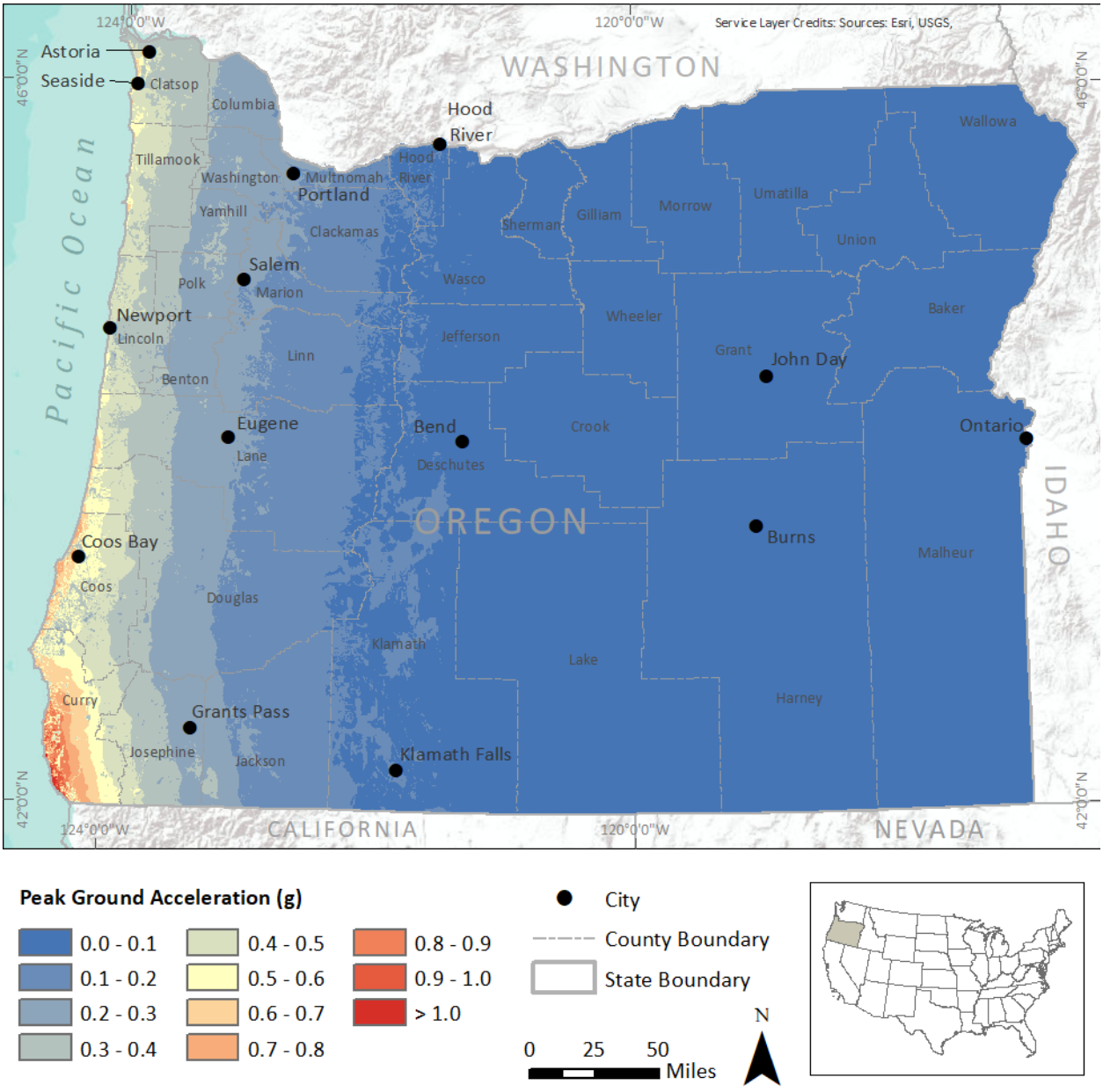

4.0 GROUND DEFORMATION MAPS

4.1 Liquefaction

Madin and Burns (2013) used GIS models to implement the methods described in the Hazus-MH technical manual to make a map of liquefaction probability and lateral spread permanent ground deformation (PGD). For this study we followed the methods of Bauer and others (2020) and use Hazus-MH to calculate a lookup table for the liquefaction hazard values. A Hazus-MH input model was created with one entry for each combination of PGA (in 0.01-g increments) and liquefaction susceptibility class. When Hazus-MH loss estimation is calculated for these input data, the output is a table that includes liquefaction probability and lateral spread deformation values for all possible combinations of ground shaking and liquefaction susceptibility. The PGA and liquefaction susceptibility rasters are then joined to the lookup table to produce a final raster for liquefaction probability and lateral spread deformation. This approach provides results that are consistent and compatible with Hazus-MH and incorporates the new high-resolution coseismic geohazard data.

In addition to PGA and liquefaction susceptibility, Hazus-MH requires a value for depth to water table and characteristic magnitude. We use 5 ft (1.52 m) for depth to water, assuming fully saturated and hence worst-case condition. The choice of magnitude is more complicated. Both liquefaction probability and lateral spread ground deformation are a function of PGA and the duration of shaking, and Hazus-MH uses correction factors (see FEMA, 2011, Figures 4.7, 4.10) that depend on the magnitude of the earthquake responsible for most of the shaking. West of the Cascades, 2% probabilistic shaking is dominated by Mw ~9 Cascadia subduction earthquakes. East of the Cascades, the 2% probabilistic shaking is dominated by local crustal faults and background seismicity with maximum magnitudes of ~ 7. This is apparent in deaggregation diagrams for the 2% probabilistic data, as shown in **Figure 4-1**. The 2% probabilistic hazard for Ashland on the west side of the Cascades is almost entirely due to Cascadia earthquakes, while the hazard in Klamath Falls on the east is almost entirely due to crustal earthquakes. We can therefore calculate a lookup table for each magnitude and apply those values in the parts of the state corresponding to the appropriate dominant magnitude. We used the Wirth and others (2021) Cascadia ensemble ground motion to guide the division of the state by selecting all values greater than 0.10 g, and using the eastern edge of that zone to draw a smooth boundary that largely coincides with the crest of the Cascades (**Figure 4-2**). The value of 0.10 g closely approximates the threshold used by Hazus-MH (see FEMA, 2011, Table 4-13) for the onset of liquefaction (0.09 g), so the Cascadia ensemble event is unlikely to cause liquefaction farther east. East of this boundary we used a lookup table based on an Mw 7 earthquake, and to the west we used the Mw 9 event. The resulting liquefaction probability and lateral spread deformation maps for the 2% probabilistic shaking are shown in **Figure 4-3**.

Figure 4-1. Comparison of 2% probabilistic shaking deaggregation for Ashland (above) and Klamath Falls (below). Position of bars shows the distance of the rupture (rRup) from the site and magnitude of earthquakes contributing to the probabilistic shaking, and the height of the bar represents the amount each source contributes to the total hazard. Hazard in Klamath Falls is dominated by nearby moderate earthquakes, and in Ashland by very large Cascadia subduction events. Data from USGS Unified Hazard Tool, https://earthquake.usgs.gov/hazards/interactive/

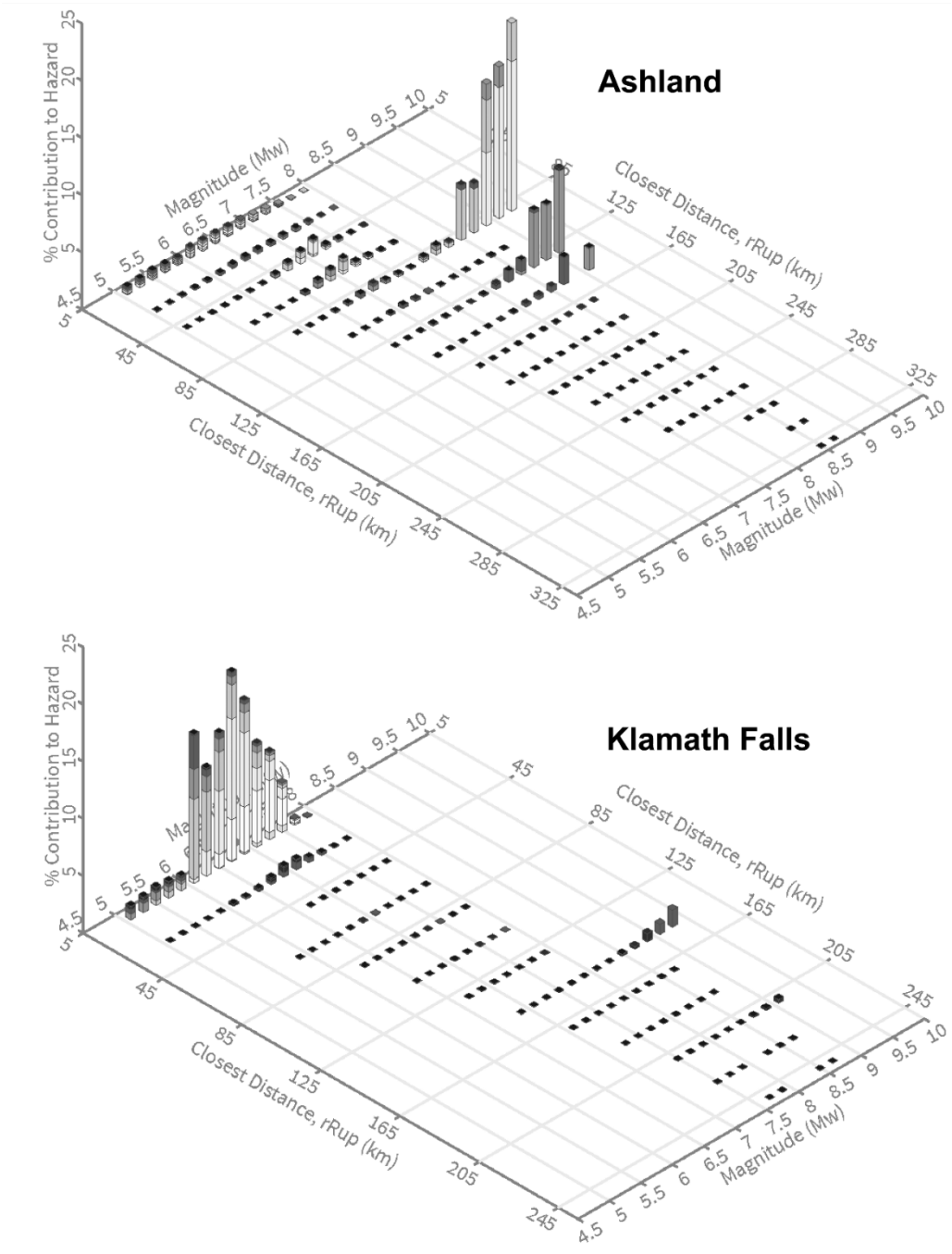

Figure 4-2. Characteristic magnitude boundary between areas using Mw 9 and Mw 7 lookup tables.

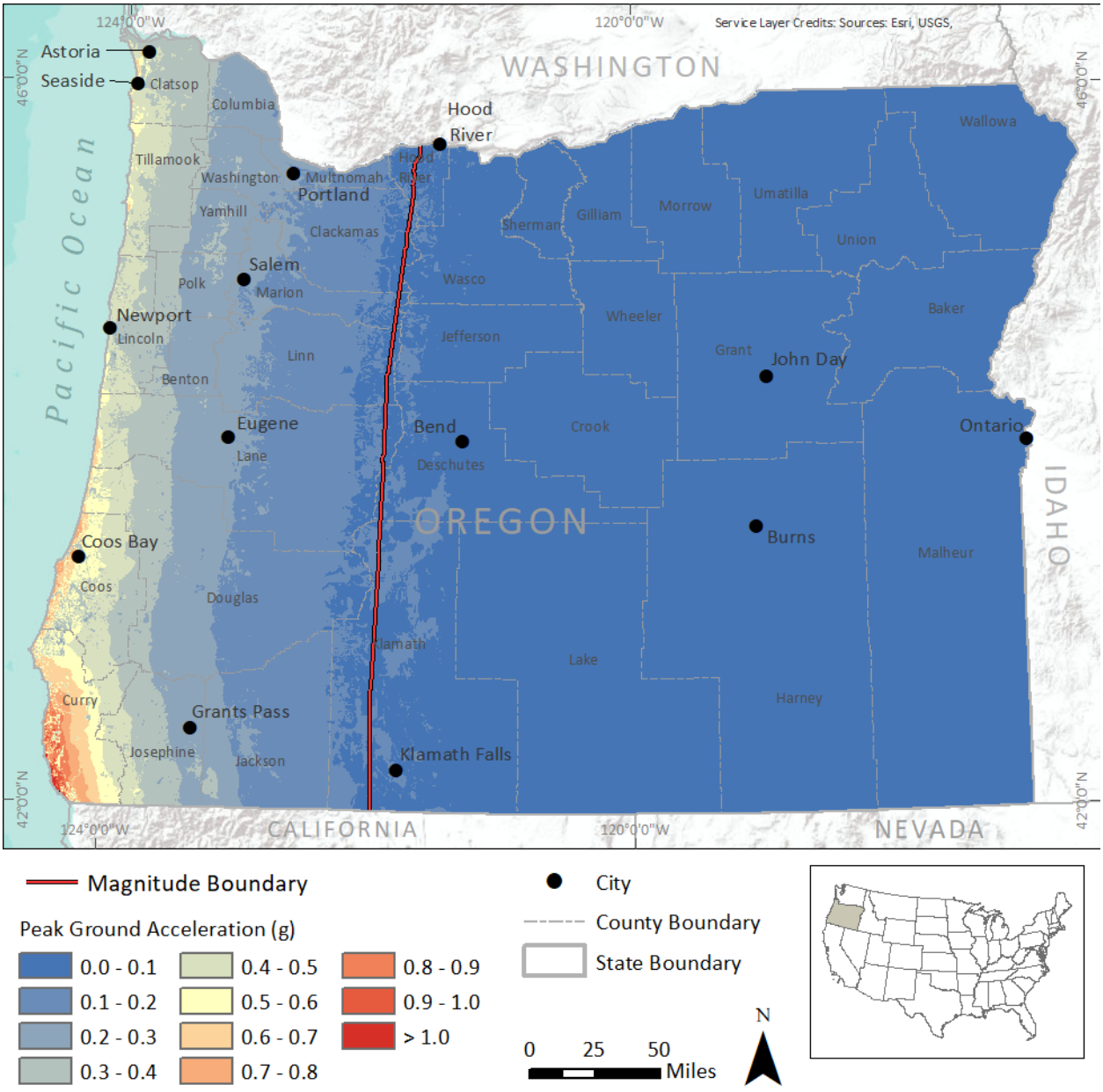

Figure 4-3. Liquefaction probability and lateral spread PGD for the 2% probabilistic shaking model.

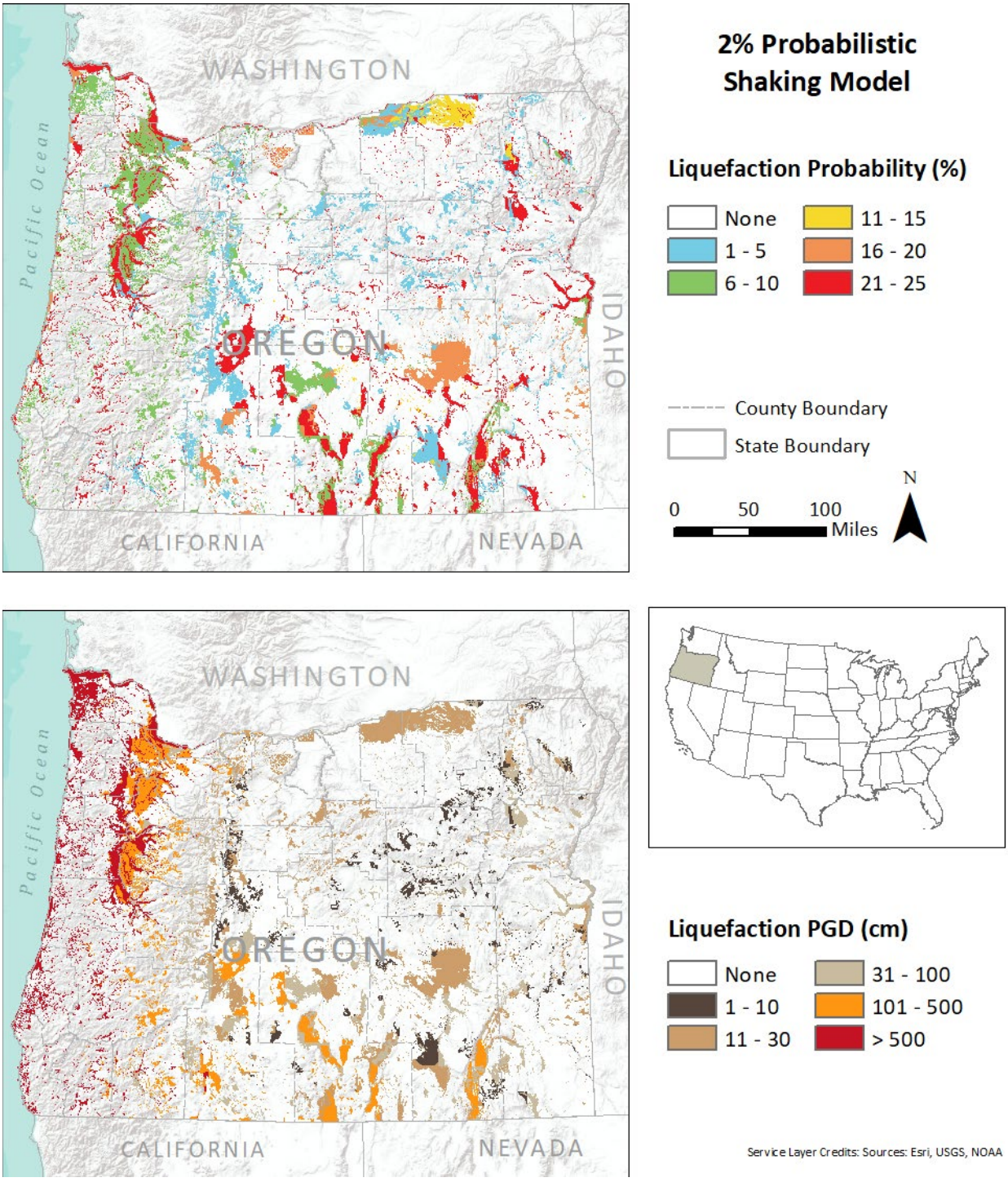

For the Cascadia ensemble shaking model, a single lookup table was used with Mw 9 as the characteristic magnitude. The resulting liquefaction probability and lateral spread deformation maps are shown in **Figure 4-4**.

Figure 4-4. Liquefaction probability and lateral spread PGD for the Cascadia ensemble shaking model.

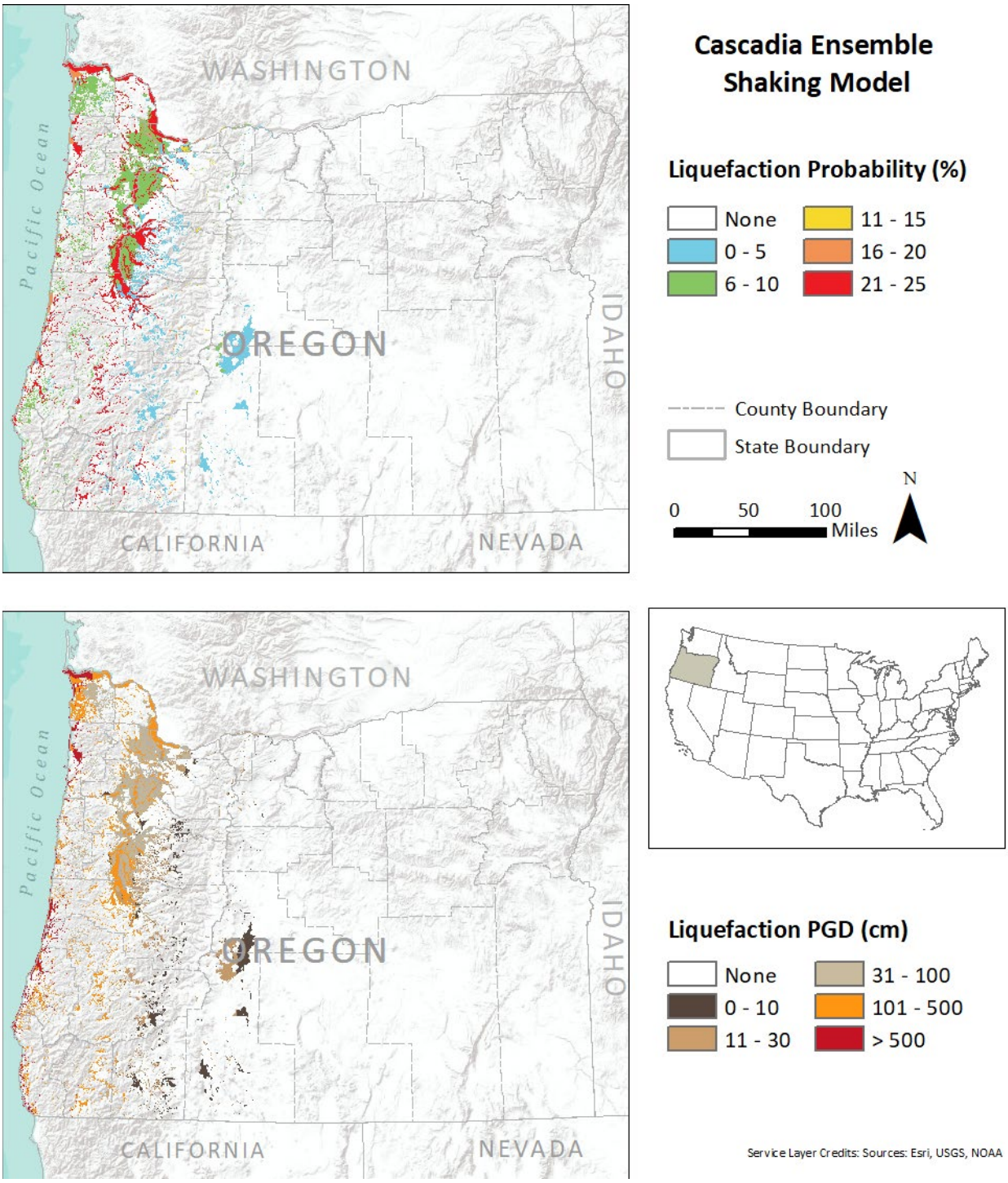

4.2 Earthquake-induced landslides

As described above for liquefaction, we ran Hazus-MH with input tables for both an Mw 7 and an Mw 9 earthquake that included all combinations of values for PGA (at 0.01-g increments) and landslide susceptibility. The output from Hazus-MH included values for landslide probability and permanent ground deformation for all combinations in a lookup table. The lookup table was then joined to the maps of PGA and wet or dry landslide susceptibility to create maps of landslide probability and ground deformation for both wet and dry soil conditions. As with liquefaction, landslide permanent ground deformation is sensitive to the magnitude chosen for the Hazus-MH calculation, which uses a relationship between magnitude and number of shaking cycles (FEMA, 2011, Hazus-MH, Table 4.13). The state was again divided as described in section 4.1 and separate lookup tables were used for Mw 9 west of the Cascades and for Mw 7 to the east. This division is reasonable because the value of 0.10 g is the critical acceleration for landslide susceptibility class IX, which means that only areas with susceptibility of X would potentially be triggered to the east of the boundary. The site PGA east of this boundary everywhere exceeds 0.05 g, the threshold for landslides in susceptibility Category X, so this is an appropriate boundary for the two areas of influence. As with liquefaction we simply used the Mw 9 lookup table for the landslide probability and PGD maps using the Cascadia ensemble model. The resulting landslide probability and ground deformation maps are shown in **Figure 4-5** and **Figure 4-6** (2% probabilistic) and **Figure 4-7** and **Figure 4-8** (Cascadia ensemble model).

Figure 4-5. Dry condition landslide probability and PGD maps for the 2% probabilistic model.

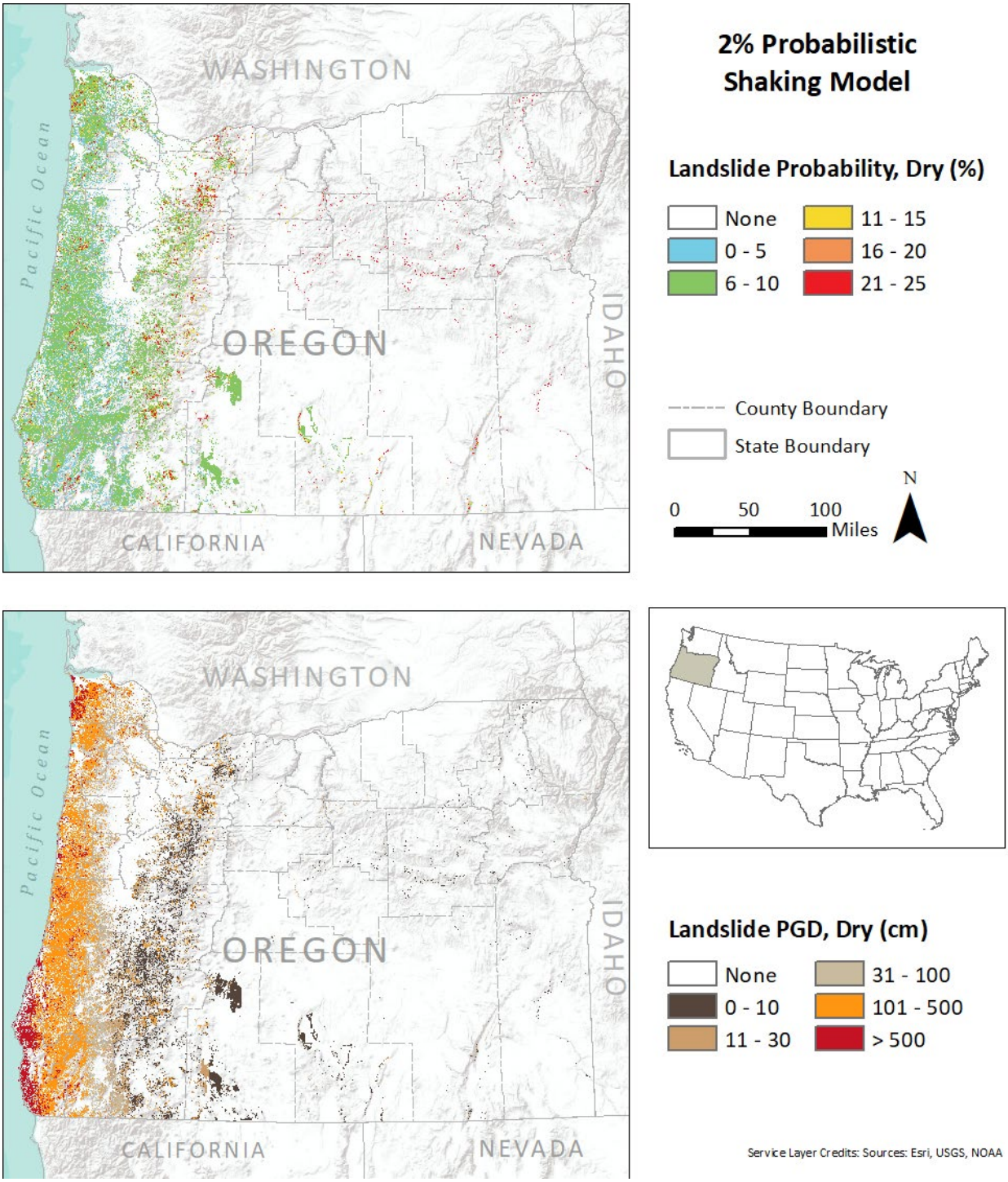

Figure 4-6. Wet condition landslide probability and PGD maps for the 2% probabilistic model.

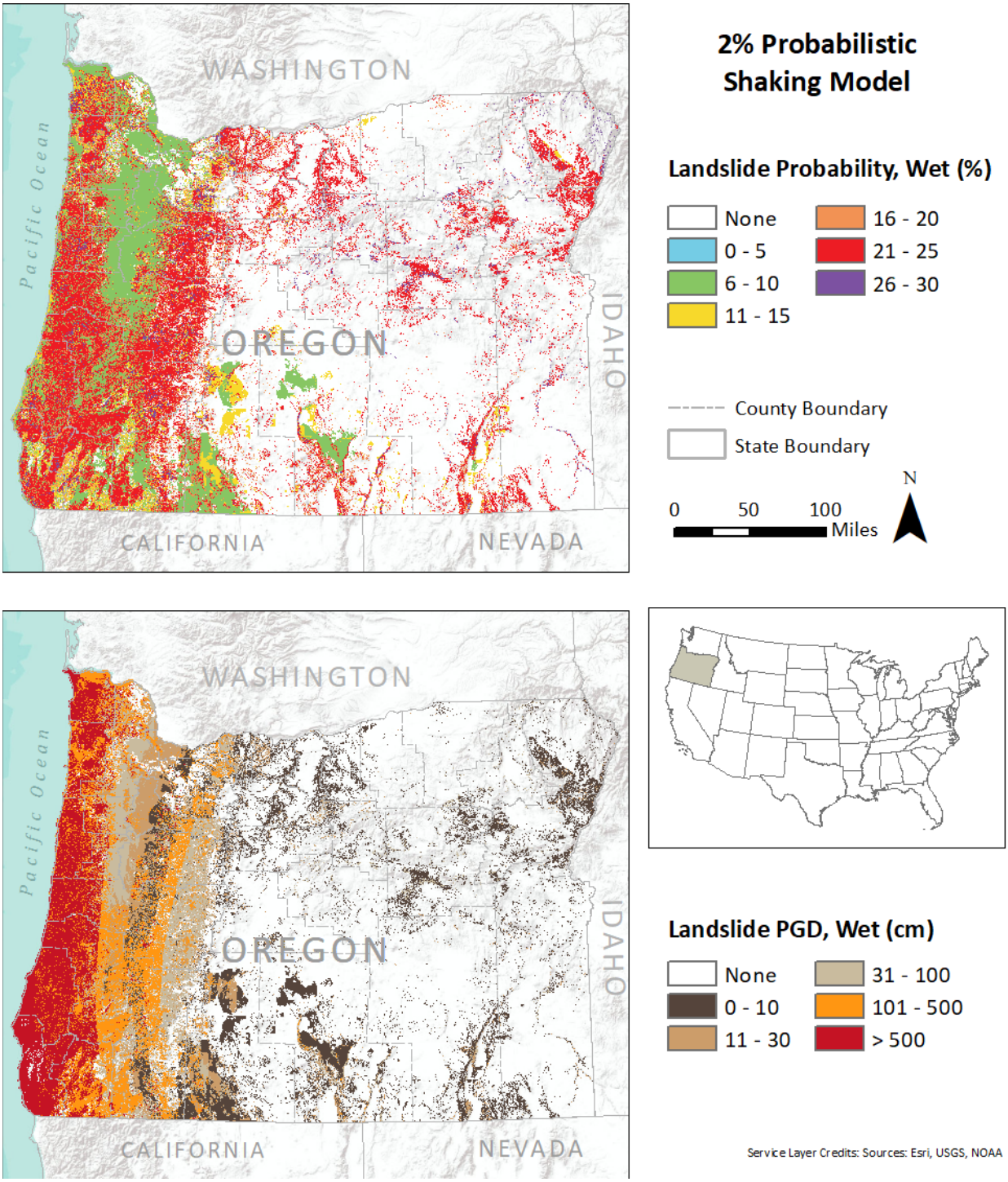

Figure 4-7. Dry condition landslide probability and PGD maps for the Cascadia ensemble model.

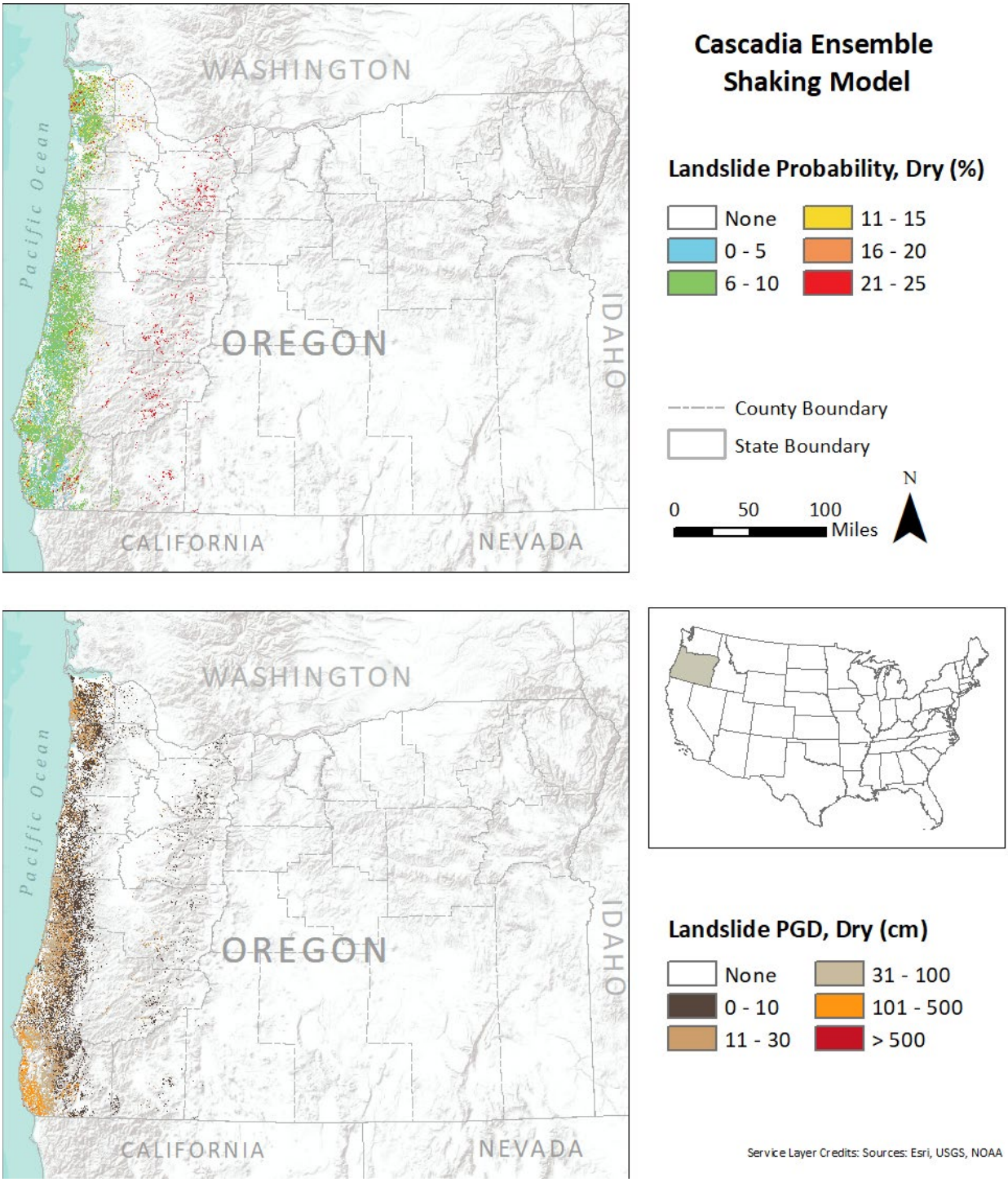

Figure 4-8. Wet condition landslide probability and PGD maps for the Cascadia ensemble model.

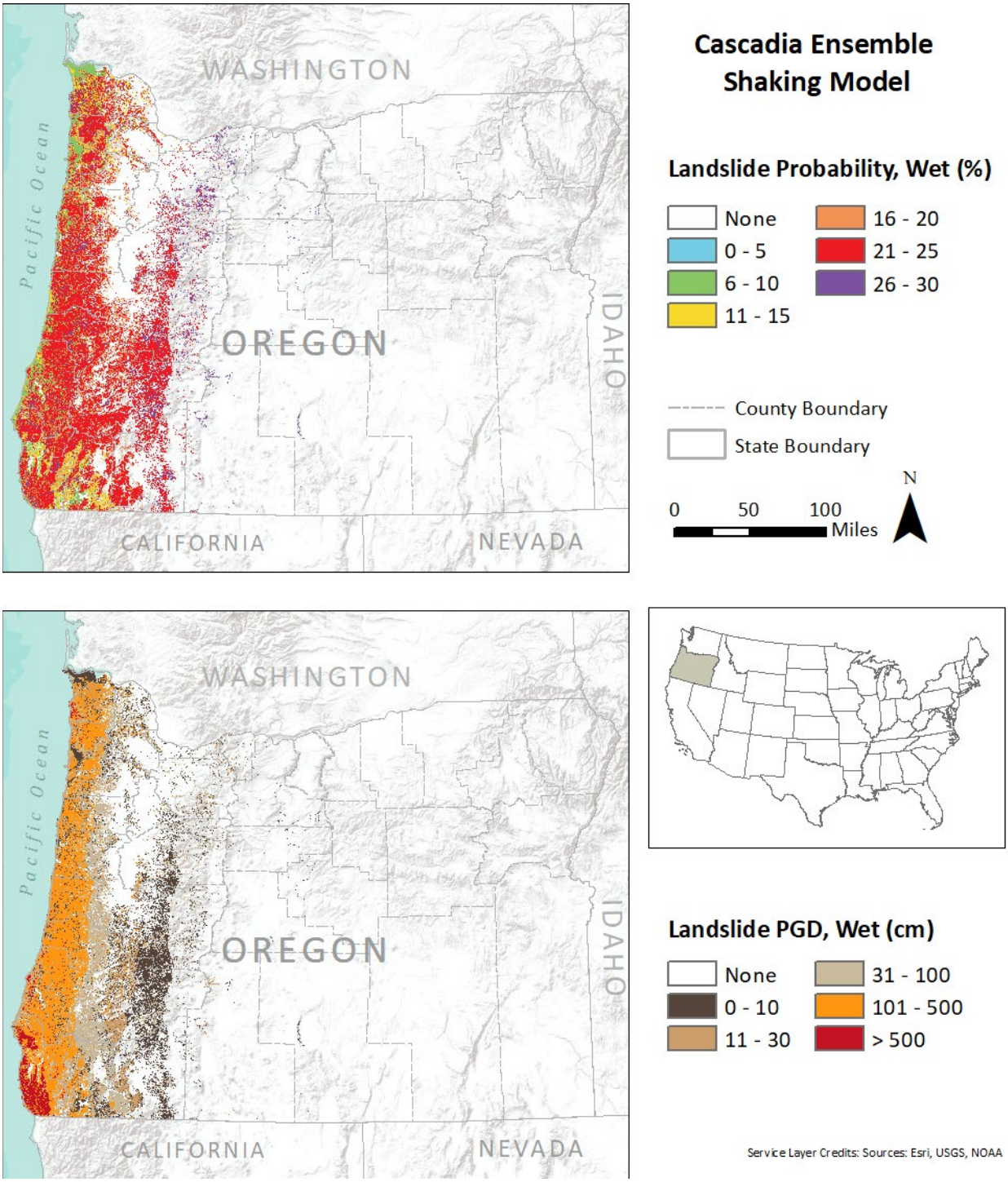

5.0 OTHER HAZARD MAPS

5.1 Instrumental intensity map

The maps of projected ground shaking in this report are useful for loss estimations in Hazus-MH and for other similar regional hazard assessments. However, the parameters the maps describe are based on quantitative values recorded by seismographs and are difficult for non-specialists to interpret. To provide hazard information that is useful to a broader audience, we include a map of projected instrumental intensity. Earthquake intensity, typically using the Modified Mercalli Intensity scale (MMI) (USGS, 2021), measures the strength of an earthquake on the basis of its qualitative effects on people, objects, and structures (**Figure 5-1**). An instrumental intensity map (Worden and others, 2020) relates quantitative earthquake shaking values based on recorded or modeled ground shaking to Modified Mercalli Intensity values to provide a map that shows earthquake shaking using commonly understood terms (**Figure 5-2**). To make the map, we used the PGV values from the 2% probabilistic and Cascadia ensemble ground motion models and symbolized them following the color scheme given by Worden and others (2020). Although the categories are based on distinct numerical ranges of PGV, the map displays a gradation of color representing each class rather than sharp boundaries. This is meant to emphasize the fact that the intensity values have significant uncertainty and that the earthquake effects themselves are gradational. Users can determine the exact instrumental intensity class by querying the GIS data for the respective PGV map. The two instrumental intensity maps are provided as Plates 1 and 2.

Figure 5-1. Modified Mercalli Intensity scale (modified from U.S. Geological Survey, 2021a, b).

Intensity Scale	Effects on People	Effects on Objects	Effects on Buildings	Effects on Environment
I	Felt only by very few under especially favorable conditions.			
II	Felt by a few at rest, especially on upper floors of buildings.	Delicately suspended objects may swing.		
III	Felt by some indoors, especially on upper floors of buildings, vibrations similar to passing of a truck, duration estimated.	Parked cars may rock slightly, hanging objects may swing appreciably.		
IV	Felt indoors by many, outdoors by few, some awakened at night. Sensation like heavy truck striking building.	Dishes, windows, and doors disturbed, parked cars rock noticeably.	Walls creak, windows rattle.	
V	Felt by nearly everyone, many awakened, frightens a few.	Pictures swing, some dishes and windows broken, unstable objects overturned.	Some cracked walls and windows.	Trees and bushes noticeably shaken.
VI	Felt by all, many frightened, some move unsteadily.	Many objects fall from shelves; some heavy furniture moved.	Damage slight, some fallen plaster, broken windows, and damaged chimneys.	Some fall of tree limbs and tops, isolated rockfalls, landslides, and liquefaction.
VII	Frightens most; some lose balance.	Heavy furniture overturned.	Damage negligible in buildings of good design and construction; slight to moderate damage in well-built ordinary structures; considerable damage in poorly-built structures, weak chimneys broken at roofline, unbraced parapets fall.	Tree damage, rockfalls, landslides, and liquefaction more severe and widespread.
VIII	Many find it difficult to stand.	Fall of chimneys, factory stacks, columns, monuments, walls. Very heavy furniture moves conspicuously.	Damage slight in specially designed structures; considerable damage in ordinary substantial buildings with partial collapse. Damage great in poorly built structures.	
IX	Some forcibly thrown to the ground.		Damage considerable in specially designed structures, well-designed frame structures thrown out of plumb. Damage is great in substantial buildings, with partial collapse. Buildings shifted off foundations.	
X			Some well-built wooden structures destroyed; most masonry and frame structures destroyed with foundations. Rails bent.	

5.2 Probability of damaging shaking map

The 2% probabilistic map shows the expected maximum strength of shaking that could occur with a set probability, in this case with a 2% chance of occurring in any 50-year period. This is useful information for engineers who need to know how strong a building or other structure needs to be to withstand the worst expected earthquake in a given period, and the 2% in 50-year shaking data are the basis for most seismic design in the United States (ICC, 2021). For emergency managers, planners, lenders, insurers, homeowners, and the public, it may be more meaningful to know how likely it is that they will experience damaging shaking. Rukstales and Petersen (2019) included such a map in the data release for the 2018

USGS National Seismic Hazard maps. It uses the hazard curves that underlie the hazard maps to make a probability of potentially damaging shaking map that shows the likelihood of experiencing MMI VI shaking in the next 100 years. The 2% probabilistic model used in this report shows how the strength of shaking varies spatially at a fixed level of probability. The probability of potentially damaging shaking map shows how the probability of experiencing a fixed level of shaking varies spatially. We have used the same hazard curves to produce a probability of damaging shaking map (Plate 3) for Oregon. For each NEHRP site class, the hazard curves provide the annual probability of occurrence of 20 set levels of shaking for a wide range of spectral periods as well as PGA. We chose the threshold of damage as MMI VII (PGV value of 14 cm/s), based on the fact that building damage at MMI VI is described as "slight" whereas at MMI VII it is described as "negligible in buildings of good design and construction; slight to moderate in well-built ordinary structures; considerable damage in poorly-built or badly designed structures" (**Figure 5-1**). **Figure 5-3** shows a more detailed description of damage levels expected for higher MMI values for different building types and building contents (ABAG, 2013).

We made a raster for each NEHRP class for the SA 0.5 value corresponding to the boundary between MMI VI and VII and used our NEHRP site class map to pick values to assemble a map following the example shown in **Figure 3-1** and **Figure 3-2**. The resulting map shows the annual probability of experiencing MMI VII shaking, which we multiplied by 50 to make a final map of the chance of experiencing damaging shaking in the next 50 years. We also chose a time period of 50 years instead of 100, to better match the periods typically used for the probabilistic maps and for expressing probabilities of specific earthquakes. The range of probability for the occurrence of MMI VII shaking was divided into five classes, Very Low, Low, Medium, High, and Very High. As with the instrumental intensity map, we used a gradational color scale to emphasize the uncertain and gradational nature of the probability of damage. The probability of damaging shaking map is provided as Plate 3. There is no corresponding map for the Cascadia ensemble event because it is a scenario earthquake.

Figure 5-2. Instrumental Intensity scale (Worden and others, 2012).

PERCEIVED SHAKING	Not felt	Weak	Light	Moderate	Strong	Very strong	Severe	Violent	Extreme
POTENTIAL DAMAGE	none	none	none	Very light	Light	Moderate	Mod./Heavy	Heavy	Very Heavy
PEAK ACC.(%g)	<0.05	0.3	2.8	6.2	12	22	40	75	>139
PEAK VEL.(cm/s)	*<0.02*	*0.1*	*1.4*	*4.7*	*9.6*	*20*	*41*	*86*	*>178*
INSTRUMENTAL INTENSITY	I	II–III	IV	V	VI	VII	VIII	IX	X+

Figure 5-3. Relationship between Mercalli Intensity and building damage (ABAG, 2013).

Modified Mercalli	Building Contents	Masonry Buildings	Multi-Family Wood-Frame Buildings	1 and 2 Story Wood-Frame Buildings
VI	Some items thrown from shelves, pictures shifted, water thrown from pools.	Some walls and parapets of poorly constructed buildings crack.	Some drywall cracks.	Some chimneys are damaged, some drywall cracks. Some slab foundations, patios, and garage floors slightly crack.
VII	Many items are thrown from walls and shelves. Furniture shifts.	Poorly constructed buildings are damaged and some well-constructed buildings crack. Cornices and unbraced parapets fall.	Plaster cracks, particularly at inside corners of buildings. Some soft-story buildings strain at the first floor level. Some partitions deform.	Many chimneys are broken and some collapse, damaging roofs, interiors, and porches. Weak foundations can be damaged.
VIII	Nearly everything is thrown down from shelves, cabinets, and walls. Furniture overturned.	Poorly constructed buildings suffer partial or full collapse. Some well constructed buildings are damaged. Unreinforced walls fall.	Soft-story buildings are displaced out of plumb and partially collapse. Loose partition walls are damaged and may fail. Some pipes break.	Unbolted houses shift off the foundation, or partially collapse if cripple walls are not braced. Structural elements (e.g. beams, joists, and foundations) are damaged. Some pipes break.
IX	Only very well anchored contents remain in place.	Poorly constructed buildings collapse. Well constructed buildings are heavily damaged. Retrofitted buildings damaged.	Soft-story buildings partially or completely collapse. Some well constructed buildings are damaged.	Poorly constructed buildings are heavily damaged, some partially collapse. Some well constructed buildings are damaged.
X	Only very well anchored contents remain in place.	Retrofitted buildings are heavily damaged, and some partially collapse.	Many well constructed buildings are damaged.	Well constructed buildings are damaged.

6.0 DISCUSSION

The data provided in this initial version of the Oregon Seismic Hazard Database are intended to update and expand upon the previous statewide earthquake hazard data provided by Madin and Burns (2013). Several layers are newly added here, but there are substantial differences between this study and Madin and Burns (2013) where the layers are directly comparable. The most important differences are described and explained in this section.

6.1 Differences between Cascadia M9 shaking maps

As described in the introduction, the fundamental difference between the Madin and Burns (2013) shaking map and the Cascadia ensemble map is that the ensemble map shows the median values from a suite of simulations with varying parameters instead of values from a single simulation. **Figure 6-1** shows the difference between the two Cascadia shaking models for PGA, in which positive values are areas where the Cascadia ensemble shaking is stronger than the Madin and Burns (2013) shaking. Over most of the state, the differences are within 0.02 g, indicating little difference. There are broad areas of along the coast where the Cascadia ensemble model is significantly higher, due to differences the calculation methods and source parameters, which lead to differences in bedrock shaking. In the Willamette Valley and Tualatin Basin there are differences of 0.05 to 0.1 g, which are associated with areas underlain by alluvial deposits and Missoula flood deposits. The Missoula flood deposits have higher shaking in the ensemble model, which is the result of differences in how site amplification is calculated. The areas underlain by alluvial deposits have lower shaking in the ensemble model, which is due to the change in NEHRP site class (**Table 2-3**) from D to E, and the way that the ensemble model calculates site amplification. In the ensemble model, Class E soils de-amplify PGA, PGV, and SA 03 significantly at higher shaking levels. This results in significantly lower shaking in the ensemble models for all areas with NEHRP class E, which includes alluvial and colluvial deposits and landslides. Landslides and alluvial deposits are very common, so areas of lower ensemble model shaking are common in **Figure 6-1**. The lower shaking does not mean that the hazard is necessarily lower, as alluvial deposits are assigned to the highest liquefaction susceptibility class and landslides are assigned to the most susceptible landslide material class (**Table 2-2**).

Large areas in the Cascades show a significant increase in shaking in the ensemble map, which is due to the re-assignment of glacial deposits from NEHRP class C to D (**Table 2-3**).

Figure 6-1. Comparison of Cascadia ensemble and Madin and Burns (2013) Cascadia maps for PGA, as a difference—positive values (warm colors) occur where the ensemble model is higher..

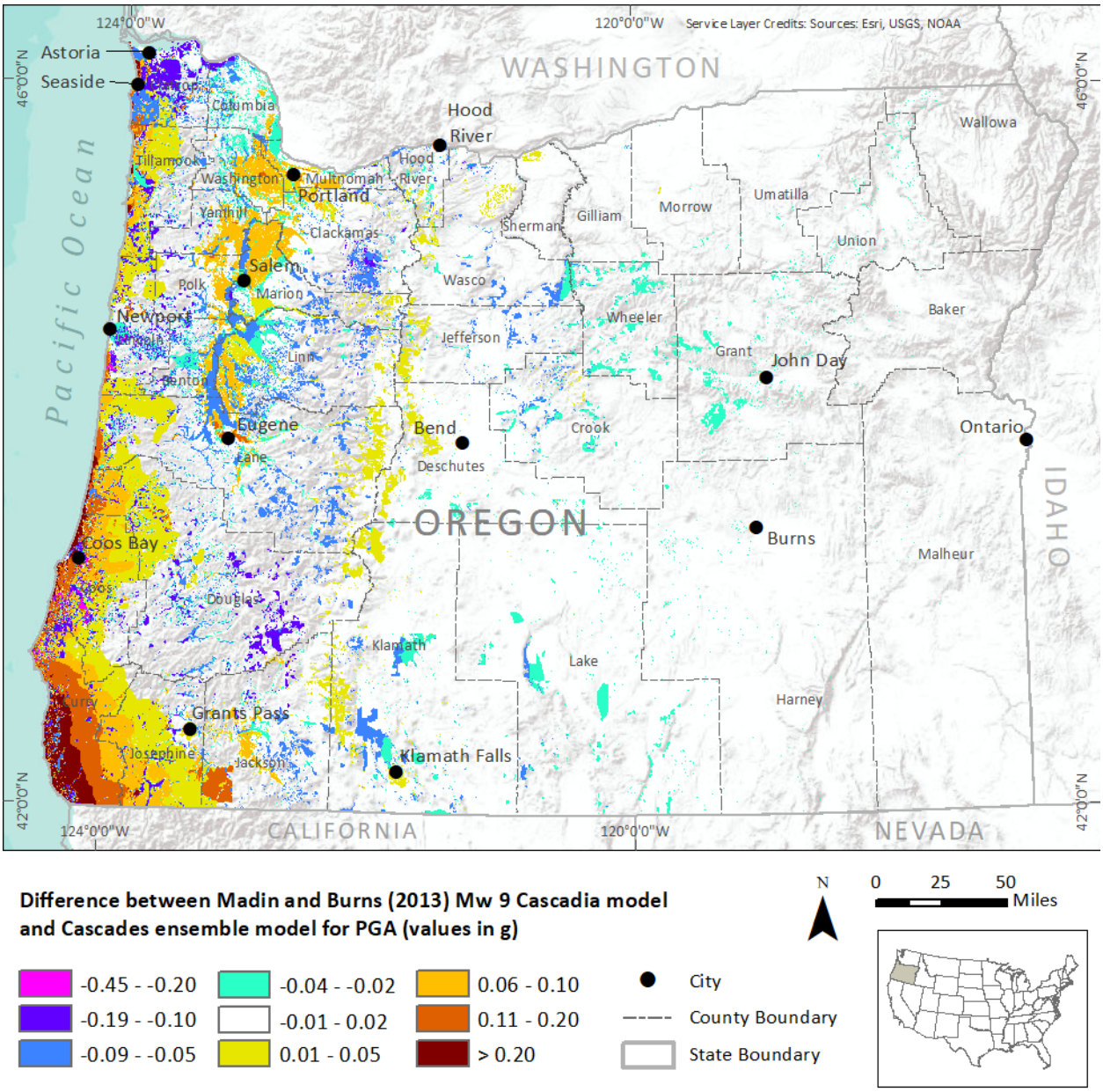

6.2 Differences between the Cascadia ensemble and 2% probabilistic maps

The comparison between the Cascadia ensemble and 2% probabilistic maps is complicated. The Cascadia ensemble map represents variations on a single event with no information about the frequency of occurrence over time. The 2% probabilistic map represents all possible earthquake sources with information about the frequency of occurrence of earthquakes from each source as a central parameter. A direct comparison may not be meaningful for planning or engineering purposes but is valuable because the 2% probabilistic is everywhere much higher, apparently conflicting with the widely held perception that a Cascadia Mw 9 is the "big one" (Schulz, 2015). **Figure 6-2** compares the Cascadia ensemble and 2% probabilistic PGA maps as a ratio, showing that for most of western Oregon the 2% probabilistic is 2-3 times as high as the Cascadia ensemble. There are two reasons why the 2% probabilistic is so much higher than the ostensible "big one" represented by the Cascadia ensemble. First, the 2% probabilistic includes many other sources that may locally shake stronger than a Cascadia Mw 9 event. These events may be much less frequent, but the 2% in 50 year probability level is equivalent to an earthquake recurrence time of 2,475 years. The second reason is that the Cascadia ensemble map shows the median value of shaking, while the 2% probabilistic is nominally showing the 98th percentile of possible shaking.

Figure 6-2 also illustrates the fact that the Cascadia ensemble map is not meaningful east of the Cascade Range, where the 2% probabilistic map is 3 to 10 times higher. Thus, the 2% probabilistic provides consistent hazard information for the entire state.

Figure 6-2. Comparison of the 2% probabilistic and Cascadia ensemble maps for PGA, as a ratio.

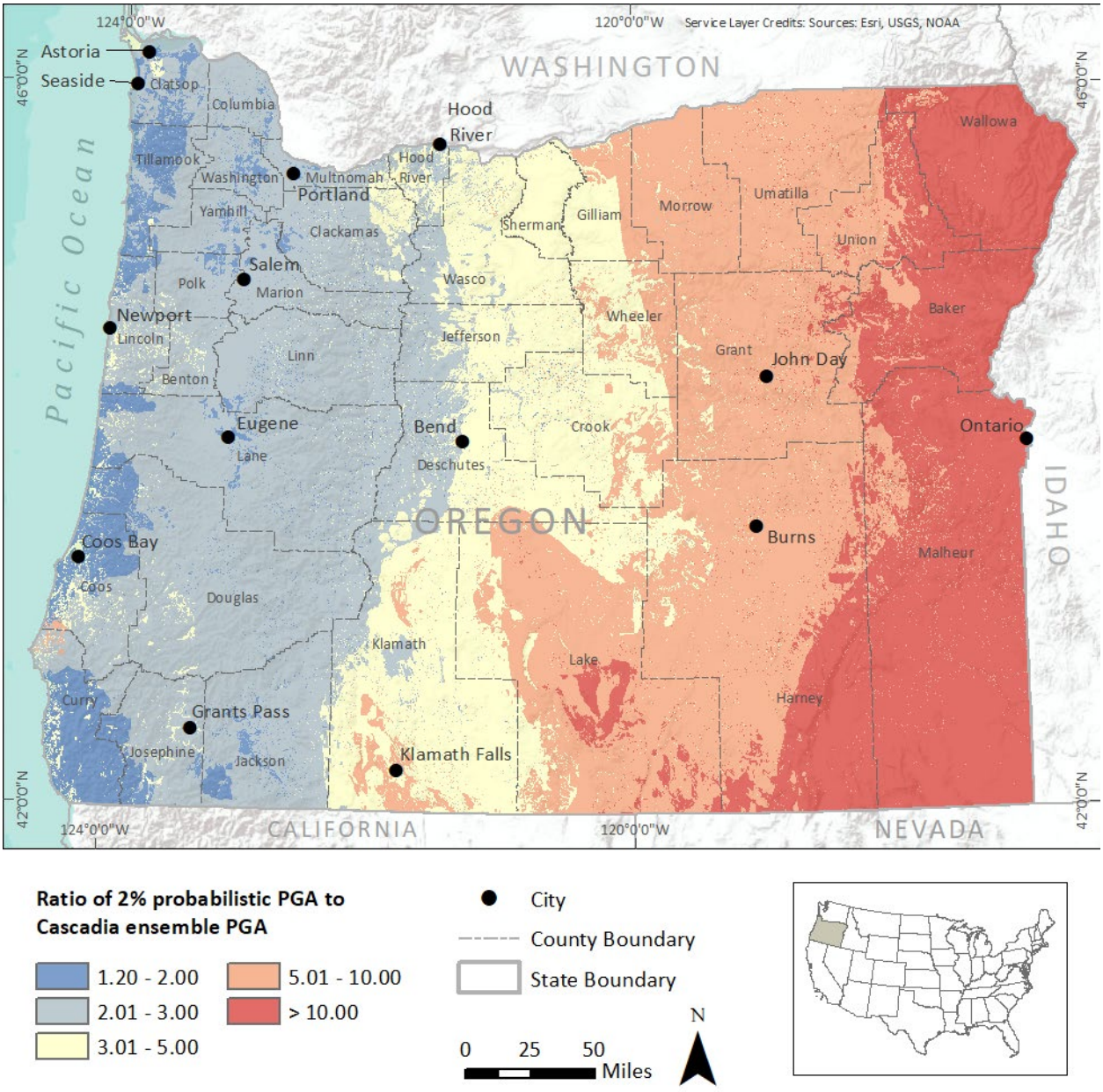

6.3 Differences between liquefaction and landslide probability and PGD maps

There are large differences between the landslide PGD maps for the Madin and Burns (2013) Cascadia model and the maps derived from the Cascadia ensemble model. Madin and Burns (2013) provided only a wet condition landslide PGD map; there is no comparison for the dry PGD maps. The largest differences occur at the extreme end of the modeled displacement range. For displacement less than 100 cm the maps are very similar, with a mean value of 30 cm (1σ = 169 cm) for nonzero values. However, for all nonzero values less than 500 cm, the Madin and Burns (2013) map has a mean of 199 cm (1σ = 331 cm) and a maximum value of 3,567 cm, while the Cascadia ensemble map has a mean of 118 cm (1σ = 169 cm) and a maximum value of 2,669 cm. Although there are some differences in the underlying landslide susceptibility maps due to the addition of new mapping and reassignment of values for some units, the primary source of the difference is in the calculation methods. Madin and Burns (2013) implemented the calculations described in the Hazus-MH technical manual (FEMA, 2011), while the Cascadia ensemble maps were calculated directly by Hazus-MH, as described in section 5.2. There were significant ambiguities in the description of the calculations in the Hazus-MH technical manual (FEMA, 2011), which we assume are responsible for this discrepancy. One term, which relates the number of shaking cycles to moment magnitude (equation 4-26 and Figure 4.13 in the Hazus-MH technical manual (FEMA, 2011) appears to be based on earthquakes no larger than Mw 8.5, so the extrapolation of the formula to Mw 9 is probably inaccurate. Another key term is the displacement factor or distance moved in each shaking cycle at a given ratio of induced acceleration to critical acceleration (FEMA, 2011, Figure 4.14). No formula was provided for this relationship, so the values were interpolated directly from the graph in the figure. There may also be other differences between how Hazus-MH calculates these values and the method used by Madin and Burns (2013) that contribute to the discrepancy but addressing those was beyond the scope of this study.

7.0 ACKNOWLEDGMENTS

This project was funded by the Oregon Geospatial Enterprise Office through its Framework Data Development Program under Interagency Agreement DASPS-3350-19. We are very grateful to Alex Grant and Erin Moriarty at the USGS for their willingness to run custom versions of their Cascadia ensemble model for this project and their patience with our requests for revisions. We thank Bill Burns and Jonathan Allan of DOGAMI for their thorough and constructive reviews.

8.0 REFERENCES

Association of Bay Area Governments (ABAG), 2013, Making sense of the Modified Mercalli Intensity scale — a measure of shaking, https://abag.ca.gov/sites/default/files/making_sense_of_the_modified_mercalli_intensity_scale.pdf, accessed 1/21/21.

Appleby, C.A., Burns, W.J., Hairston-Porter, R.W., and Bauer, J.M., 2019, Coseismic landslide susceptibility, liquefaction susceptibility, and soil amplification class maps, Clackamas, Columbia, Multnomah, and Washington Counties, Oregon: For use in Hazus: FEMA's methodology for estimating potential losses from disaster; Oregon Department of Geology and Mineral Industries Open-File Report O-19-09, https://www.oregongeology.org/pubs/ofr/p-O-19-09.htm.

Bauer, J.M., Burns, W.J., and Madin, I.P., 2018, Earthquake regional impact analyses for Clackamas, Multnomah and Washington Counties: Oregon Department of Geology and Mineral Industries Open-File Report O-18-02, https://www.oregongeology.org/pubs/ofr/p-O-18-02.htm.

Bauer, J.M., Cakir, R., Allen, C., Mickelson. K., Contreras, T., Hairston-Porter, R., and Wang, Y., 2020, Earthquake Regional Impact Analysis for Columbia County, Oregon and Clark County, Washington. Oregon Department of Geology and Mineral Industries Open-File Report O-20-01, https://www.oregongeology.org/pubs/ofr/p-O-20-01.htm.

Black, G.L., Wang, Z., Wiley, T.J., and Priest, G.R., 2000, Relative earthquake hazard map of the Klamath Falls metropolitan area, Klamath County, Oregon: Oregon Department of Geology and Mineral Industries Interpretive Map 19; zipped file: https://www.oregongeology.org/pubs/ims/IMS-019.zip.

Bommer, J.J., and Alarcon, J.E., 2006, The prediction and use of peak ground velocity: Journal of Earthquake Engineering, v. 10, no. 1, 1–31.

Burns, W. J., 2007, Comparison of remote sensing datasets for the establishment of a landslide mapping protocol in Oregon. AEG Special Publication 23: Vail, Colo., Conference Presentations, 1st North American Landslide Conference.

Burns, W.J., and Madin, I.P., 2009, Protocol for inventory mapping of landslide deposits from light detection and ranging (lidar) imagery: Oregon Department of Geology and Mineral Industries, Special Paper 42, 30 p., geodatabase template, https://www.oregongeology.org/pubs/sp/p-SP-42.htm.

Calhoun, N.C., Burns, W.J., and Franczyk, J.J., 2020, Landslide hazard and risk study of Tillamook County, Oregon: Oregon department of Geology and Mineral Industries Open-File Report O-20-13, https://www.oregongeology.org/pubs/ofr/p-O-20-13.htm.

Federal Emergency Management Agency (FEMA), 2011, Hazus-MH MH 2.0, Multi-Hazard Loss Estimation Methodology software and documentation.

Federal Emergency Management Agency (FEMA), 2015, 2015 NEHRP recommended seismic provisions for new buildings and other structures, Vol. I: Part 1, Provisions; Part 2, Commentary: Washington, D.C., Building Seismic Safety Council of the National Institute of Building Sciences, FEMA P-1050-1, https://www.fema.gov/media-collection/nehrp-recommended-seismic-provisions-new-buildings-and-other-structures-2015.

Franczyk, J.J., Madin, I.P., Duda, C.J.M., and McClaughry, J.D., 2020a, Oregon geologic data compilation [OGDC], release 7 (statewide): Oregon Department of Geology and Mineral Industries Digital Data Series, https://www.oregongeology.org/pubs/dds/p-OGDC-7.htm.

Franczyk, J.J., Burns, W. J., and Calhoun, N.C., 2020b, Statewide Landslide Information Database for Oregon release 4.2 Oregon Department of Geology and Mineral Industries, https://www.oregongeology.org/slido/index.htm.

Goldfinger, C., and others, 2012, Turbidite event history: Methods and implications for Holocene paleoseismicity of the Cascadia Subduction Zone: U.S. Geological Survey Professional Paper 1661-F, https://doi.org/10.3133/pp1661F.

Goldfinger, C., Galer, S., Beeson, J., Hamilton, T., Black, B., Romsos, C., Patton, J., Nelson, C.H., Hausmann, R., and Morey, A., 2017, The importance of site selection, sediment supply, and hydrodynamics: A case study of submarine paleoseismology on the Northern Cascadia margin, Washington USA: Marine Geology, v. 384, 4–46.

Heath, D., Wald, D. J., Worden, C. B., Thompson, E. M., and Scmocyk, G., 2020, A global hybrid VS30 map with a topographic-slope-based default and regional map insets: Earthquake Spectra, v. 36, no. 3, 1570–1584.

Houston, R.A., McClaughry, J.D., Duda, C.J.M., and Niewendorp, C.A., 2018, Geologic map of the Devine Ridge North 7.5′ quadrangle, Harney County, Oregon: Oregon Department of Geology and Mineral Industries Geologic Map 121, https://www.oregongeology.org/pubs/gms/p-GMS-121.htm.

International Code Council (ICC), 2021, 2021 International Building Code: International Code Council, ICC-IBC-2021.

Madin, I.P., and Burns, W.J., 2013, Ground motion, ground deformation, tsunami inundation, coseismic subsidence, and damage potential maps for the 2012 Oregon Resilience Plan for Cascadia Subduction Zone Earthquakes; Oregon Department of Geology and Mineral Industries Open-File Report O-13-06, https://www.oregongeology.org/pubs/ofr/p-O-13-06.htm.

Madin, I.P., and McClaughry, J.D., 2019, Geologic map of the Biggs Junction and Rufus 7.5' quadrangles, Sherman and Gilliam Counties, Oregon, Oregon Department of Geology and Mineral Industries Geologic Map 124, https://www.oregongeology.org/pubs/gms/p-GMS-124.htm.

Madin, I.P., and Wang, Z., 1999a, Relative earthquake hazard maps for selected urban areas in western Oregon: Canby-Barlow-Aurora, Lebanon, Silverton-Mount Angel, Stayton-Sublimity-Aumsville, Sweet Home, Woodburn-Hubbard: Oregon Department of Geology and Mineral Industries Interpretive Map 8, https://www.oregongeology.org/pubs/ims/p-ims-008.htm.

Madin, I.P., and Wang, Z., 1999b, Relative earthquake hazard maps for selected urban areas in western Oregon: Dallas, Hood River, McMinnville-Dayton-Lafayette, Monmouth-Independence, Newburg-Dundee, Sandy, Sheridan-Willamina, St. Helens-Columbia City-Scappoose: Oregon Department of Geology and Mineral Industries Interpretive Map 7, https://www.oregongeology.org/pubs/ims/p-ims-007.htm.

Madin, I.P., and Wang, Z., 1999c, Relative earthquake hazard maps for selected urban areas in western Oregon: Ashland, Cottage Grove, Grants Pass, Roseburg, Sutherlin-Oakland: Oregon Department of Geology and Mineral Industries Interpretive Map 9, https://www.oregongeology.org/pubs/ims/p-ims-009.htm.

Madin, I.P., and Wang, Z., 1999d, Relative earthquake hazard maps for selected coastal communities in Oregon: Astoria-Warrenton, Brookings, Coquille, Florence-Dunes City, Lincoln City, Newport, Reedsport-Winchester Bay, Seaside-Gearhart-Cannon Beach, Tillamook: Oregon Department of Geology and Mineral Industries Interpretive Map 10, https://www.oregongeology.org/pubs/ims/p-ims-010.htm.

McClaughry, J.D., Duda, C.J.M., and Ferns, M.L., 2019, Geologic map of the Poison Creek and Burns 7.5′ quadrangles, Harney County, Oregon: Oregon Department of Geology and Mineral Industries Geological Map Series GMS 123, 127 p., 2 pl., scale 1:24,000, Esri format geodatabase; shapefiles, metadata; spreadsheet (4 sheets), https://www.oregongeology.org/pubs/gms/p-GMS-121.htm.

McClaughry, J.D., Scott, W.E., Duda, C.J.M., and Conrey, R.M., 2020a, Geologic map of the Dog River and northern part of the Badger Lake 7.5' quadrangles, Hood River County, Oregon: Oregon Department of Geology and Mineral Industries Geologic Map 126, 1:24,000, https://www.oregongeology.org/pubs/gms/p-GMS-126.htm.

McClaughry, J.D., Duda, C.J.M., and Ferns, M.L., 2020b, Geologic map of the Burns Butte 7.5′ quadrangle, Harney County, Oregon: Oregon Department of Geology and Mineral Industries Geological Map 125, 168 p., 1 pl., scale 1:24,000, Esri format geodatabase; shapefiles, metadata; spreadsheet (4 sheets), https://www.oregongeology.org/pubs/gms/p-GMS-125.htm.

McClaughry, J.D., Herinckx, H.H., Niewendorp, C.A., Azzopardi, C.J.M., and Hackett, J.M., 2021, Geologic map of the Dufur area, Wasco County, Oregon: Oregon Department of Geology and Mineral Industries Geological Map 127, 209 p., 3 pl., scale 1:24,000, Esri format geodatabases (3); shapefiles, metadata; spreadsheets (16 sheets), https://www.oregongeology.org/pubs/gms/p-GMS-127.htm.

McClaughry, J.D., Ferns, M.L., and Gordon, C.L., in press, Geology of the north half of the lower Crooked River basin, Crook, Deschutes, Jefferson, and Wheeler Counties, Oregon: Oregon Department of Geology and Mineral Industries, 1 pl., scale 1:63,360, Esri format geodatabase; shapefiles, metadata; spreadsheet.

Niewendorp, C.A., Duda, C.J.M., Houston, R.A., and McClaughry, J.D., 2018, Geologic map of the Devine Ridge South 7.5′ quadrangle, Harney County, Oregon: Oregon Department of Geology and Mineral Industries Geological Map 120, https://www.oregongeology.org/pubs/gms/p-GMS-120.htm.

Oregon Seismic Safety Policy Advisory Commission (OSSPAC), 2013, The Oregon Resilience Plan: reducing risk and improving recovery for the next Cascadia earthquake and tsunami, Oregon Seismic Safety Policy Advisory Commission Salem, Oregon, 341 p., https://www.oregon.gov/oem/documents/oregon_resilience_plan_final.pdf.

Petersen, M.D., and others, 2019, The 2018 update of the US National Seismic Hazard Model: Overview of model and implications: Earthquake Spectra, v. 36, no. 1, 5–41, https://doi.org/10.1177/8755293019878199.

Rukstales, K.S., and Petersen, M.D., 2019, Data release for 2018 update of the U.S. National Seismic Hazard Model: U.S. Geological Survey data release, https://doi.org/10.5066/P9WT5QVB.

Schulz, K., 2015, The really big one; New Yorker Magazine, July 20, 2015 issue, https://www.newyorker.com/magazine/2015/07/20/the-really-big-one.

Shumway, A.M., Clayton, B.S., and Rukstales, K.S., 2020, Data release for additional period and site class data for the 2018 National Seismic Hazard Model for the Conterminous United States (ver. 1.1, February 2020): U.S. Geological Survey data release, https://doi.org/10.5066/P9RQMREV.

U.S. Geological Survey (USGS), 2021a, The Modified Mercalli Intensity (MMI) scale assigns intensities as ... [web page], https://www.usgs.gov/media/images/modified-mercalli-intensity-mmi-scale-assigns-intensities, accessed 1/21/21.

U.S.Geological Survey (USGS), 2021b, https://www.usgs.gov/media/images/modified-mercalli-intensity-scale , accessed 5/28/21.

Wang, Y., and Leonard, W.J., 1995, Relative earthquake hazard maps of the Salem East and Salem West quadrangles, Marion and Polk Counties, Oregon: Oregon Department of Geology and Mineral Industries Geologic Map 105, https://www.oregongeology.org/pubs/gms/GMS-105.zip.

Wang, Y., and Priest, G.R., 1995, Relative earthquake hazard maps of the Siletz Bay area, Lincoln County, Oregon: Oregon Department of Geology and Mineral Industries Geologic Map 93, https://www.oregongeology.org/pubs/gms/GMS-093.zip.

Wells, R.E., and others, 2020, Geologic map of the greater Portland metropolitan area and surrounding region, Oregon and Washington: U.S. Geological Survey Scientific Investigations Map 3443, pamphlet 55 p., 2 sheets, scale 1:63,360, https://doi.org/10.3133/sim3443.

Wirth, E.A., Grant, A., Marafi, N.A., and Frankel, A.D., 2021, Ensemble ShakeMaps for magnitude 9 earthquakes on the Cascadia Subduction Zone: Seismol. Res. Lett., v. 92, no. 1, 99–211, https://doi.org/10.1785/0220200240. [first online November 18, 2020]

Worden, C.B., Gerstenberger, M.C., Rhoades, D.A., and Wald, D.J., 2012, Probabilistic relationships between ground-motion parameters and Modified Mercalli intensity in California Bull. Seism. Soc. Am., v. 102, no. 1, 204–221, https://doi.org/10.1785/0120110156.

Worden, C.B., Thompson, E.M., Hearne, M., and Wald, D.J., 2020, ShakeMap Manual Online: technical manual, user's guide, and software guide, U. S. Geological Survey. http://usgs.github.io/shakemap/. https://doi.org/10.5066/F7D21VPQ.

Youd, T.L., and Perkins, D. M., 1978, Mapping liquefaction-induced ground failure potential: J. Geotech. Eng. Div., 104, 433–446.

9.0 APPENDIX: OSHD-1.0 DATABASE LAYERS

The Oregon Seismic Hazard Database, release 1 (OSHD-1.0), file name OSHD Release 1_0.gdb, contains the following:

- Data Source Map
  - OSHD_1_Data_Source_Map
- Coseismic Geohazard Maps
  - NEHRP_Site_Class_Map
  - Liquefaction_Susceptibility_Map
  - Landslide_Geologic_Group_Map
  - Dry_Landslide_Susceptibility_Map
  - Wet_Landslide_Susceptibility_Map
- Cascadia Subduction Zone Mw 9 Ensemble Maps
  - CSZE_PGA_Map
  - CSZE_PGV_Map
  - CSZE_SA03_Map
  - CSZE_SA10_Map
  - CSZE_Liquefaction_PGD_Map
  - CSZE_Liquefaction_Probability_Map
  - CSZE_Wet_Landslide_PGD_Map
  - CSZE_Wet_Landslide_Probability_Map
  - CSZE_Dry_Landslide_PGD_Map
  - CSZE_Dry_Landslide_Probability_Map
  - CSZE_Instrumental_Intensity_Map
- 2% in 50-year (2,475-year) Probabilistic Maps
  - P2475_PGA_Map
  - P2475_PGV_Map
  - P2475_SA03_Map
  - P2475_SA10_Map
  - P2475_Liquefaction_PGD_Map
  - P2475_Liquefaction_Probability_Map
  - P2475_Wet_Landslide_PGD_Map
  - P2475_Wet_Landslide_Probability_Map
  - P2475_Dry_Landslide_PGD_Map
  - P2475_Dry_Landslide_Probability_Map
  - P2475_Instrumental_Intensity_Map
- Probability_of_Damaging_Shaking_Map